Cellular/Molecular

Multiple Conductances Cooperatively Regulate Spontaneous Bursting in Mouse Olfactory Bulb External Tufted Cells

Shaolin Liu and Michael T. Shipley
Department of Anatomy and Neurobiology, Program in Neuroscience, University of Maryland School of Medicine, Baltimore, Maryland 21201

External tufted (ET) cells are juxtaglomerular neurons that spontaneously generate bursts of action potentials, which persist when fast synaptic transmission is blocked. The intrinsic mechanism of this autonomous bursting is unknown. We identified a set of voltage-dependent conductances that cooperatively regulate spontaneous bursting: hyperpolarization-activated inward current (I_h), persistent Na^+ current (I_{NaP}), low-voltage-activated calcium current ($I_{L/T}$) mediated by T- and/or L-type Ca^{2+} channels, and large-conductance Ca^{2+}-dependent K^+ current (I_{BK}). I_h is important in setting membrane potential and depolarizes the cell toward the threshold of I_{NaP} and $I_{T/L}$, which are essential to generate the depolarizing envelope that is crowned by a burst of action potentials. Action potentials depolarize the membrane and induce Ca^{2+} influx via high-voltage-activated Ca^{2+} channels (I_{HVA}). The combined depolarization and increased intracellular Ca^{2+} activates I_{BK}, which terminates the burst by hyperpolarizing the membrane. Hyperpolarization activates I_h and the cycle is regenerated. A novel finding is the role of L-type Ca^{2+} channels in autonomous ET cells bursting. A second novel feature is the role of BK channels, which regulate burst duration. I_L and I_{BK} may go hand-in-hand, the slow inactivation of I_L requiring I_{BK}-dependent hyperpolarization to deactivate inward conductances and terminate the burst. ET cells receive monosynaptic olfactory nerve input and drive the major inhibitory interneurons of the glomerular circuit. Modulation of the conductances identified here can regulate burst frequency, duration, and spikes per burst in ET cells and thus significantly shape the impact of glomerular circuits on mitral and tufted cells, the output channels of the olfactory bulb.

Key words: **external tufted cells; bursting mechanism; persistent Na^+ current; hyperpolarization-activated nonselective cation current; low-threshold activated Ca^{2+} current; large-conductance calcium-dependent K^+ current**

Introduction

Oscillatory or rhythmic brain activity underlies many physiological functions including sleep-wakefulness, arousal, motivation, memory, cognition, and sensory and motor processing (Laurent, 2002; Buzsaki and Draguhn, 2004). In the olfactory system, odors evoke both fast and slow network oscillations in the olfactory bulb (Laurent, 2002). Oscillations in the slower-theta frequency range are related to exploratory sniffing (Lledo et al., 2005; Wilson and Mainen, 2006). The patterned sensory input resulting from active "theta sniffing" may establish olfactory bulb oscillations that enhance odor processing (Young and Wilson, 1999). Rhythmic oscillations can also be driven by intrinsic bursting of pacemaker neurons. Recently, a subpopulation of neurons in the glomerular layer, external tufted (ET) cells, were found to spontaneously generate rhythmic bursts of action potentials (Hayar et al., 2004a). ET cells could, therefore, function as pacemaker neurons in the olfactory network.

ET cells differ from most other pacemaker neurons in which bursting depends on network synaptic activity (Ramirez et al., 2004). ET cell bursting persists, and indeed becomes more regular, when fast synaptic events are pharmacologically eliminated. Such autonomous, network-independent bursting has been reported for only a few kinds of mammalian neurons including cells in the pre-Bötzinger complex (Ramirez et al., 2004), hippocampal CA3 pyramidal cells (Hablitz and Johnston, 1981), ventral hippocampal dentate granule cells (Jinno et al., 2003), and cerebellar Purkinje cells (Womack and Khodakhah, 2004).

Although much remains to be learned about the physiological impact of ET cell bursting, some features are known. ET cells respond optimally to rhythmic, sniffing-related input. Each ET cell has its own intrinsic or "native" burst frequency when isolated from synaptic input. The bursting frequencies of the ET cell population are limited to a relatively narrow spectrum ranging from ~0.2 to 10 Hz (Hayar et al., 2004a), which is nearly identical with the spectrum of normal breathing-sniffing frequencies exhibited by rats and mice. Each ET cell is entrained by repetitive olfactory nerve (ON) stimulation at all frequencies higher than the intrinsic frequency of the cell. Consequently, as the frequency of ON synaptic input increases, more ET cells are entrained such that the population bursts more synchronously. Synchrony is further augmented by electrical coupling among ET cells of the same glomerulus (Hayar et al., 2005). ET cells receive monosynaptic input from ON and relay odorant information to other postsynaptic elements in the glomeruli including the majority of

Received Aug. 27, 2007; revised Dec. 18, 2007; accepted Dec. 18, 2007.

This work was supported by National Institutes of Health Grant DC005676. We thank Dr. Bradley Alger for critical comments on this manuscript and Dr. Adam Puche for assistance in data analysis.

Correspondence should be addressed to Michael T. Shipley, Department of Anatomy and Neurobiology, Program in Neuroscience, University of Maryland School of Medicine, 20 Penn Street, Baltimore, MD 21201. E-mail: mshipley@umaryland.edu.

DOI:10.1523/JNEUROSCI.3906-07.2008

 0270-6474/08/281625-15$15.00/0

periglomerular (PG) cells and all short axon (SA) cells of the same glomerulus (Hayar et al., 2004b). Thus, frequency-dependent synchronous ET cell bursting may potently regulate the impact of sensory signals on olfactory bulb output neurons.

The present study aims to elucidate the intrinsic mechanism of the unusual capacity of ET cell to generate autonomous bursting activity. Knowledge of the ionic conductances that regulate ET cell bursting should allow its experimental manipulation and advance our understanding of ET cell roles in glomerular network function and olfactory coding.

Materials and Methods

Olfactory bulb slices from 5- to 6-week-old male C57BL/6J mice were prepared as previously described (Hayar et al., 2004a). Briefly, horizontal slices (300 μm) were cut with a Leica (Nussloch, Germany) VT1000s vibratome in an ice-cold and oxygenated (95% O_2–5% CO_2) sucrose-based artificial CSF (sucrose-aCSF) containing the following (in mM): 220 sucrose, 3 KCl, 1.25 NaH_2PO_4, 2.6 $MgSO_4$, 26 $NaHCO_3$, 10 glucose. After 30 min incubation in normal aCSF at 30°C, slices were then transferred to aCSF at room temperature until they were used for experiments. Normal aCSF was continuously bubbled with 95% O_2–5% CO_2 and had the following composition (in mM): 124 NaCl, 3 KCl, 1.25 NaH_2PO_4, 1.3 $MgSO_4$, 1.3 $CaCl_2$, 26 $NaHCO_3$, 10 glucose. During experiments, slices were perfused at 3 ml/min with aCSF equilibrated with 95% O_2–5% CO_2 and warmed to 30°C.

Electrophysiological recordings were made from olfactory bulb ET cells visualized using BX50WI (Olympus, Tokyo, Japan) fixed-stage upright microscope equipped with near-infrared differential interference contrast optics. Additional physiological criteria were used to further confirm ET cell identity (Hayar et al., 2004a) (see Results), and in some cases ET cell identity was morphologically confirmed by biocytin filling and immunostaining. Current or voltage signals were recorded with a MultiClamp 700B amplifier (Molecular Devices, Palo Alto, CA). Patch recording electrodes were pulled from standard-wall glass capillary tubes without filament (WPI, Sarasota, FL). For voltage-clamp calcium-current experiments, electrodes (3–4 MΩ) were filled with an internal solution containing 5.5 mM EGTA, 0.5 mM $CaCl_2$, 95 mM Cs-methanesulfonate, 20 mM tetraethylammonium (TEA)-Cl, 10 mM HEPES, 3 mM Mg-ATP, 0.3 mM Na-GTP, 10 mM Tris-phosphocreatine, 0.1% biocytin. For current-clamp recordings, patch pipettes (4–7 MΩ) contained 5.5 mM EGTA, 0.5 mM $CaCl_2$, 110 mM K-gluconate, 5.5 mM $Mg\text{-}Cl_2$, 10 mM HEPES, 3 mM Na_2-ATP, 0.3 mM Na_3-GTP, 10 mM Tris-phosphocreatine, 0.1% biocytin. In the experiments with low EGTA intracellular solution shown in Figure 1, *F*, *H*, and *I*, pipette solution contained the following (in mM): 110 K-gluconate, 17.5 KCl, 4 NaCl, 4 $MgCl_2$, 10 HEPES, 0.2 EGTA, 3 Mg-ATP, 0.3 Na_2-GTP, 10 Tris-phosphocreatine, 0.1% biocytin. Osmolarity of all pipette solutions for whole-cell patch-clamp recording was adjusted to 285–295 mOsm, pH to 7.3 with KOH or CsOH.

The liquid junction potential (11–13 mV) was not corrected. Access resistance was typically $<$20 MΩ and routinely compensated by 70–80% in voltage-clamp experiments. Input resistance was measured under voltage clamp with a 30 ms, 5 mV hyperpolarization from a holding potential of $-$55 mV.

Voltage or current records were low-pass filtered at 4 kHz and sampled at 10 kHz with a DIGIDATA 1322A 16-bit analog-to-digital converter (Molecular Devices) using Clampex 9.2 (Molecular Devices). Data were analyzed with Clampfit 9.2 (Molecular Devices), Origin 7.5 (Origin Lab, Northampton, MA), and a custom script-program written in NeuroExplorer (Nex Technologies, Littleton, MA), which was used to measure the minimal membrane potential (MMP), average membrane potential (AMP), and duration of depolarizing envelope. MMP was measured as the nadir of the membrane potential after each burst. AMP was measured from continuous traces of depolarizing envelopes on which the action potentials were truncated at $-$45 mV (see Fig. 1*D*). A depolarizing envelope was automatically detected when the membrane depolarized from the AMP and remained depolarized for a minimum duration of 25 ms. EPSPs have a shorter ($<$15 ms) duration and would not detected as envelopes by the software. Nevertheless, all glutamatergic, ionotropic EPSPs were eliminated in this study by 1,2,3,4-tetrahydro-6-nitro-2,3-dioxo-benzo[*f*]quinoxaline-7-sulfonamide disodium salt (NBQX) and DL-2-amino-5-phosphonovaleric acid (APV). The envelope duration was measured as the time difference between the two points in each envelope where the membrane potential crosses the AMP (see Fig. 1*D*,*E*). To calculate the burst frequency, the interburst interval was measured as the time difference between the peaks of the first action potentials from consecutive bursts (see Fig. 1*E*). All data are presented as mean $\pm$ SEM. Statistical significance was determined using the Student's *t* test, with a significance level of $p < 0.05$.

The biocytin-filled cells were developed as previously described (Hayar et al., 2004a). Briefly, the paraformaldehyde-fixed slices were embedded in 10% gelatin and sectioned at 50 μm thickness. The sections were subsequently reacted with 0.3% H_2O_2, 0.3% Triton X-100, ABC complex, and Ni-DAB chromagen. After dehydration, the sections were mounted in DPX (a mixture of distyrene, tricresyl phosphate, and xylene). Two-dimensional reconstructions of filled neurons were made with Neurolucida software (MicroBrightField, Colchester, VT).

All drugs diluted in aCSF were delivered to slices by bath application. NBQX, APV, and gabazine (SR95531), 4-ethylphenylamino-1,2-dimethyl-6-methylaminopyrimidinium chloride [ZD7288 (ZD)], (−)-bicuculline methochloride, and tetrodotoxin (TTX) were purchased from Tocris Cookson (Ellisville, MO). Iberiotoxin (IBTX), ω-conotoxin MVIIC, and SNX-482 were from Peptides International (Louisville, KY). All other chemicals were purchased from Sigma (St. Louis, MO).

Results

ET cells are identified by their somatic location within the deep half of the glomerular layer having a relatively large, pear-shaped cell body with a single apical dendrite that ramifies extensively in a single glomerulus (Fig. 1*A*,*B*). Similar to rat ET cells, mouse ET cells (Fig. 1*A*,*B*) do not extend basal dendrites into the underlying external plexiform layer (EPL) and are thus distinguished from superficial tufted (ST) cells, which do have dendrites in EPL. Physiologically, ET cells are recognized by their distinctive and characteristic spontaneous bursts of action potentials superimposed on a slow depolarizing envelope (9.9 $\pm$ 0.3 mV in amplitude and 97.3 $\pm$ 2.8 ms in duration; $n = 68$); ST cells lack spontaneous bursting (Antal et al., 2006). A burst is classically defined as a cluster of two or more high-frequency action potentials, but ET cells occasionally have single spikes riding on their distinctive depolarizing envelopes. In order not to underestimate burst frequency, we defined a burst in this study as a depolarizing envelope (also referred to plateau potential) (Fig. 1*E*) that launches at least one action potential. Spontaneous ET cell bursting is resistant to a mixture of synaptic transmission blockers including NBQX (10 μM), APV (50 μM), and gabazine (10 μM) (Hayar et al., 2004a), so these drugs were used to eliminate spontaneous synaptic activity in all experiments. The oscillatory membrane potential of ET cells makes it difficult to specify their resting membrane potential, especially at high burst frequencies. To quantify ionic currents, the MMP, -55.3 ± 0.8 mV, and AMP, -51.3 ± 0.5 mV, were calculated from a 40 s recording epoch from each of 68 ET cells (Fig. 1*C*–*E*) (see Materials and Methods).

Intracellular calcium buffering stabilizes spontaneous bursting activity

Spontaneous burst firing of rat olfactory bulb ET cells runs down rapidly in whole-cell recording mode (Hayar et al., 2004a). A similar phenomenon was observed in mouse ET cells (Fig. 1*F*,*H*). Spontaneous bursting gradually decreased and then disappeared within 15 min after whole-cell break-in. The averaged decline in burst frequency from five cells over 20 min of whole-cell recording was fitted by a single exponential decay function

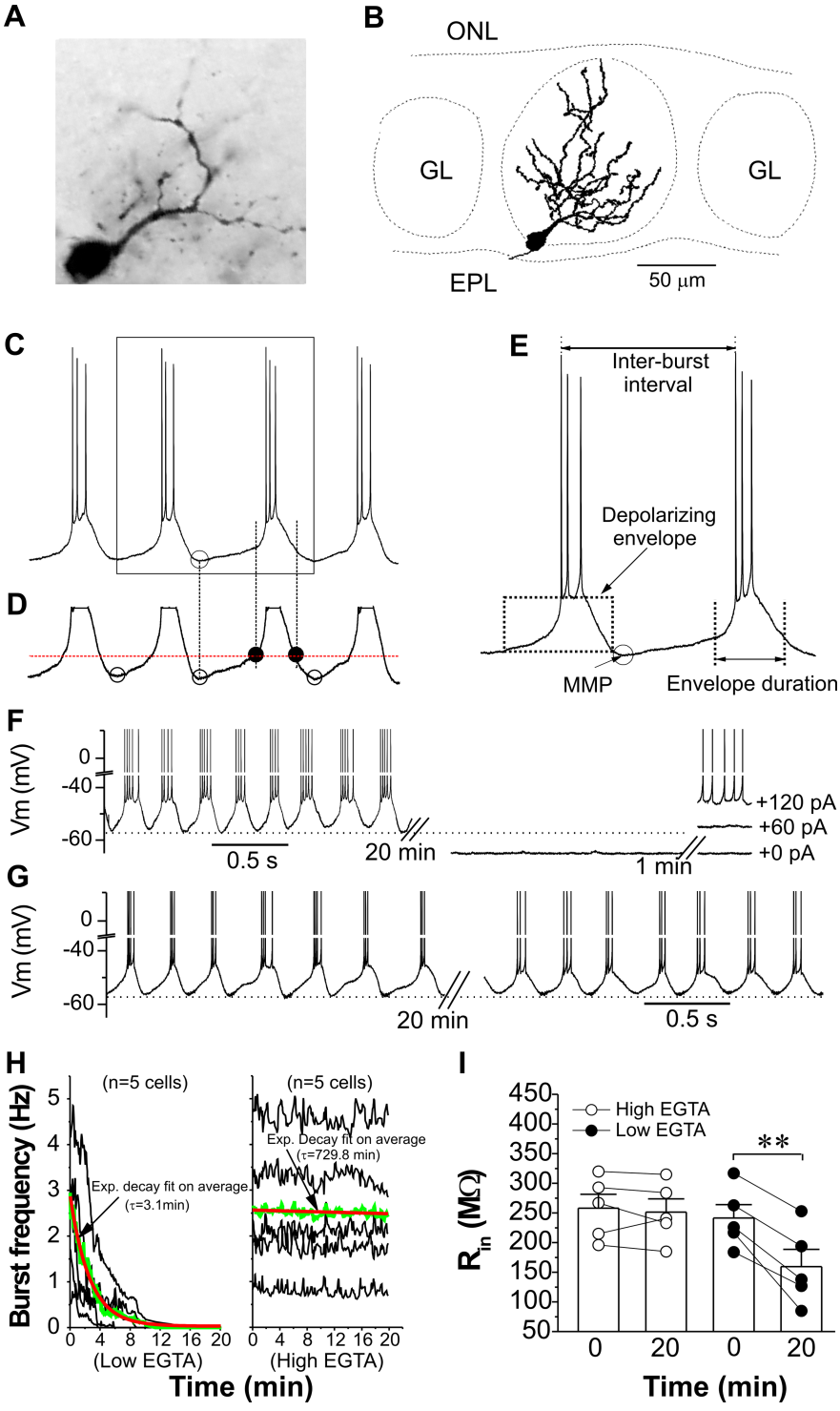

Figure 1. Bursting is stable in whole-cell recording. ***A***, Photograph of a representative mouse ET cell filled with biocytin. ***B***, Reconstruction of the cell in ***A*** (EPL, external plexiform layer; GL, glomerular layer; ONL, olfactory nerve layer). ***C***, Current-clamp recording of ET cell bursting. ***D***, Same as ***C*** with action potentials truncated at −45 mV. MMP is measured at the negative-most potential (open dots) after each burst. The AMP (red dotted line) is calculated (see Materials and Methods). Each depolarizing envelope crosses the AMP at two points (solid dots). Envelope duration is defined as the time difference between these two points. ***E***, Blowup of ***C*** showing envelope duration and interburst interval, measured as the time difference between the peaks of the first action potentials from two consecutive bursts. ***F***, ***G***, Spontaneous bursting is preserved with high (***G***) but not low (***F***) EGTA-buffered intracellular solution. ***H***, Bursting frequency was unchanged after 20 min of whole-cell recording with high internal EGTA (right graph) but was significantly reduced with low EGTA (left graph). The red lines represent the exponential decay fit of burst frequency average histograms (green) of five cells. ***I***, With low internal EGTA, input resistance is significantly reduced, whereas there is no significant change with high internal EGTA situation after 20 min whole-cell recording. Bar graphs represent averages from five cells in each condition. Error bars indicate SEM. $^{**}p < 0.01$.

with a time constant (τ) of 3.1 min. After 20 min of recording, the MMP was hyperpolarized (Fig. 1*F*) by ~10 mV (from -55.3 ± 0.5 to -65.4 ± 0.7 mV; $n = 5$; $p < 0.01$), the input resistance reduced by 35 ± 7% (Fig. 1*I*) from 241.4 ± 22.7 to 159.4 ± 29.2 MΩ ($n = 5$; $p < 0.01$) and bursting could not be restored by steady current injection. Because this rapid rundown precluded investigation of bursting mechanisms, it was necessary to obviate the problem. Intracellular Ca^{2+} buffer plays an important role in maintaining resting membrane potential and input resistance (Krnjevic et al., 1975; Milesi et al., 1999). Therefore, we increased the concentration of EGTA in the internal solution from 0.2 to 5.5 mM (see Materials and Methods) and added 0.5 mM Ca^{2+} to yield an estimated free Ca^{2+} concentration of 20 nM. Bursting activity recorded with this internal solution did not significantly change after 20 min of whole-cell recording (Fig. 1*G*,*H*). The average burst frequency from five cells decreased only from 2.6 ± 0.5 to 2.4 ± 0.5 Hz after 20 min whole-cell recording with a time constant (τ) of 729.8 min when fitted by a single exponential decay function. In addition, there was minimal change of MMP from -56.2 ± 1.7 to 57.5 ± 2.6 mV ($n = 5$; $p > 0.05$) and input resistance from 258.2 ± 23.3 to 251.6 ± 22.3 MΩ ($n = 5$; $p > 0.05$) (Fig. 1*G*,*I*). In many cases, stable bursting was maintained for >60 min. These results showed that optimal intracellular Ca^{2+} buffer prevented rundown of spontaneous bursting and suggested a Ca^{2+} dependence of bursting activity in ET cells. This internal solution was used for the remaining experiments.

Persistent Na^+ channels are active at MMP and AMP and essential for intrinsic bursting

The TTX-sensitive persistent sodium current (I_{NaP}) exists in a variety of CNS neurons (Crill, 1996). I_{NaP} is present in rat ET cells and is necessary for spontaneous burst initiation (Hayar et al., 2004a). To investigate I_{NaP} in mouse ET cells, we used a ramp protocol to depolarize the membrane from −75 to −40 mV at a velocity (30 mV/s) sufficiently slow to prevent activation of fast or transient sodium channels (I_{NaT}) (Fig. 2*A*). This protocol reliably disclosed a TTX-sensitive inward current (Fig. 2*A*). The average TTX-sensitive inward current from four cells was 13.6 ± 1.5 pA at −55.3 mV (MMP) and 42.1 ± 2.5 pA at −51.3 mV (AMP), had an activation voltage of about −60 mV, and reached its maximal magnitude (96.4 ± 7.2 pA; $n = 4$) at −45 mV (Fig. 2*B*). This shows that mouse ET

cells have an active I_{NaP} even at their MMP. This conductance increases monotonically with membrane depolarization.

To investigate the role of I_{NaP} in bursting, we treated ET cells with 1 μM TTX after a stable bursting recording was established. As shown in Figure 2*C*, in addition to hyperpolarizing the membrane from -57.4 ± 1.1 to -60.3 ± 0.9 mV ($n = 5$; $p < 0.005$), spontaneous bursting slowed and small depolarizing "humps" (arrowheads in the expanded trace) appeared between bursts. Both bursts and humps were rapidly (2.1 ± 0.2 min; $n = 5$) terminated by TTX. Low-voltage-activated (LVA) Ca^{2+} spikes could be evoked in the presence of TTX (see Figs. 6–8), but neither action potentials nor spontaneous depolarizing events were restored by depolarizing the membrane potential with steady current injection (Fig. 2*C*), indicating that I_{NaP} is required to trigger the depolarizing envelope in mouse ET cells. The presence of the small spontaneous voltage humps during early phase of 1 μM TTX application suggested that they might persist at lower concentration TTX because it takes time for the toxin to reach maximal concentration at the recorded cells. At 10 nM TTX (Fig. 2*D*), the majority of I_{NaP} (82% measured at -45 mV) (Fig. 2*D*, inset) was blocked but rebound action potentials persisted (Fig. 2*De*). Spontaneous bursting was terminated (Fig. 2*D*) and could not be restored by depolarizing current injection (Fig. 2*Dd*). Spontaneous voltage humps were again present only during the early phase of 10 nM TTX wash-in (Fig. 2*Db*) and during the late phase of washout (Fig. 2*Df*) when I_{NaP} had partially recovered (Fig. 2*D*, inset, *I–V* curve 3). This suggests that I_{NaP} is necessary to generate the humps. Although the humps were abolished (Fig. 2*Dc*) when majority of I_{NaP} was blocked by TTX, single humps could be evoked by depolarizing current steps (Fig. 2*Dd*). This indicates that the role of I_{NaP} is to depolarize the membrane to the activation voltage of Ca^{2+} currents (see below and Fig. 6), and suggests that the spontaneous humps are depolarizing envelopes that inactivate before reaching the threshold voltage required to launch action potentials.

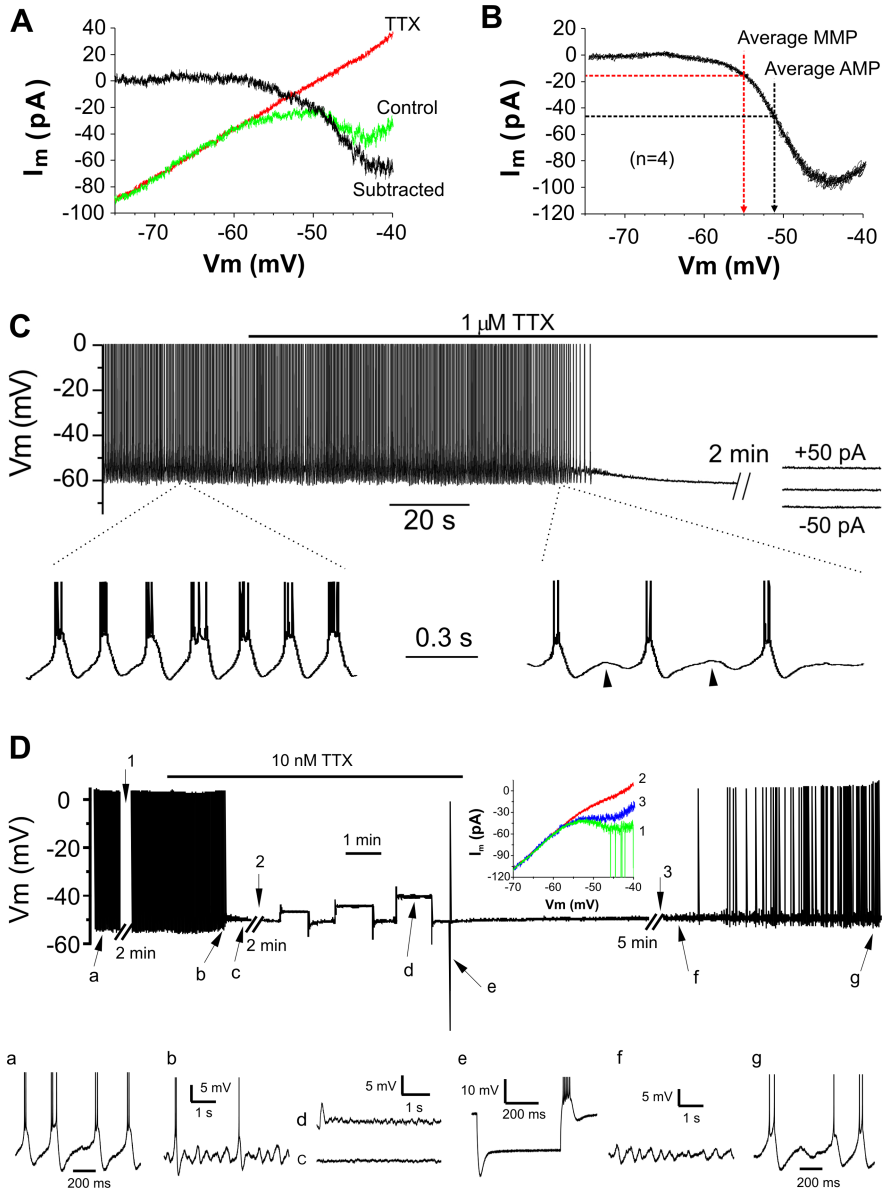

Figure 2. Persistent Na^+ current is active at minimal and average membrane potentials and is required for spontaneous bursting. ***A***, TTX-sensitive persistent Na^+ current, I_{NaP}, revealed by voltage ramp protocol from -75 to -40 mV at 30 mV/s. ***B***, Averaged *I–V* curve from four ET cells showing that I_{NaP} is active at MMP. ***C***, Bath application of TTX (1 μM) terminates the spontaneous bursting, which cannot be restored by either positive or negative steady current injection. Burst frequency declines and voltage humps (arrowheads) appear between bursts before termination (expanded traces). ***D***, Bath application of a lower concentration of TTX (10 nM; expanded traces ***a*** and ***g***) reversibly terminates the spontaneous bursting, which cannot be restored by positive steady current injection. Inset, *I–V* curves revealed by the same voltage ramp protocol as in ***A*** at different time points 1, 2, and 3. Note that 10 nM TTX significantly blocks I_{NaP} (inset, trace 2 vs trace 1) but does not block the action potentials evoked by a hyperpolarization voltage step (expanded trace ***e***). Spontaneous voltage humps only appear during the early phase of TTX wash-in (expanded trace ***b***) and late phase of washout (expanded trace ***f***) when significant I_{NaP} has been recovered (trace 3 in the inset). Only a single hump can be evoked by each depolarizing current step (expanded trace ***d***) in the presence of TTX.

I_h current contributes to setting membrane potential and is required for spontaneous bursting

The hyperpolarization-activated cation current (I_h) has been identified in a variety of mammalian neurons (Pape, 1996; Robinson and Siegelbaum, 2003). One function of I_h is to generate pacemaker activity. Of the four hyperpolarization-activated, cation-nonselective (HCN1–4) genes that encode I_h channels (Robinson and Siegelbaum, 2003) HCN2 and HCN4 mRNA are highly expressed in the olfactory bulb of rat and mouse (Montegia et al., 2000; Santoro et al., 2000), and HCN1, HCN2, and HCN3 immunoreactivity is present in glomeruli (Holderith et al., 2003; Notomi and Shigemoto, 2004). As shown in Figure 3*A*, hyperpolarizing current steps in current clamp generated depolarizing sags, indicating activation of I_h channels in ET cells. In cells voltage clamped at -55 mV, hyperpolarizing steps revealed slowly developing inward currents that were blocked by bath-applied 3 mM Cs^+ (Fig. 3*B*,*C*), a nonselective blocker of I_h channels. The amplitude of these Cs^+-sensitive inward currents steadily increased with membrane hyperpolarization from 88 ±

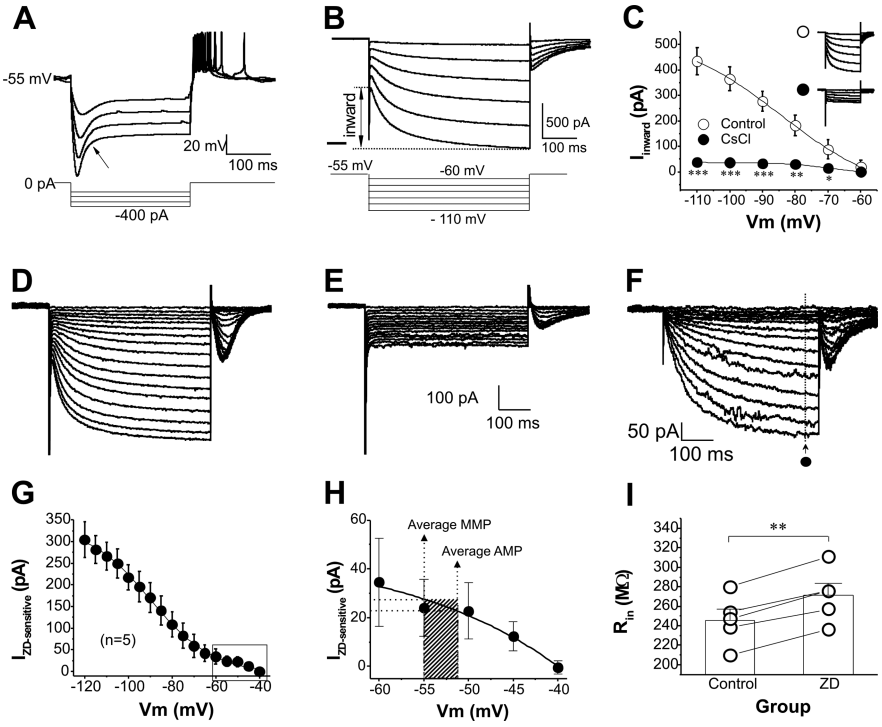

Figure 3. ET cells have a prominent I_h current that is active at MMP and AMP. ***A***, Current-clamp recording showing robust depolarizing sag (arrow) indicating the presence of I_h. ***B***, Voltage-clamp recording in the same cell in the presence of TTX (1 μM) showing hyperpolarization-activated inward current, I_h (holding potential, −55 mV). ***C***, Average *I–V* curves of I_h measured as in ***B*** with and without CsCl (3 mM in the bath; $n = 4$ cells). ***D***, Voltage-clamp recording with membrane potential hyperpolarized by voltage steps (5 mV/step) from −40 to −120 mV in the presence of TTX (1 μM). ***E***, Same cell in the presence of I_h channel blocker, ZD7288 (100 μM). ***F***, ***D*** minus ***E*** shows the ZD7288-sensitive I_h current. ***G***, *I–V* curve of steady-state ZD7288-sensitive I_h current fitted with Boltzmann equation ($n = 5$ cells). ***H***, Magnification of ***G*** in the voltage range from −60 to −40 mV, showing that there is ~25 pA of I_h active in the voltage range between MMP and AMP. ***I***, ZD7288 (100 μM) increased input resistance in all cells tested ($n = 5$) consistent with the reduction of a steady-state conductance (measured at −55 mV). Bar graphs show the averaged value from five cells. Error bars indicate SEM. *$p < 0.05$; **$p < 0.01$; ***$p < 0.001$.

37.3 pA ($n = 4$) at −70 mV to 434.5 ± 54.2 pA ($n = 4$) at −110 mV (Fig. 3*C*). The selective I_h channel blocker ZD7288 (100 μM) also blocked this current (Fig. 3*D*,*E*), confirming that it is mediated by I_h channels (Luthi et al., 1998).

To determine whether I_h contributes to setting membrane potential, ET cells were held at −40 mV and 500 ms hyperpolarizing voltage steps were used to elicit ZD7288-sensitive inward currents (Fig. 3*D–G*). When plotted against their test voltages (Fig. 3*F*,*G*), considerable ZD-sensitive currents, 23.5 pA at −51.3 mV to 28.2 pA at −55.3 mV ($n = 5$), were revealed (Fig. 3*H*), suggesting that I_h is active between MMP and AMP (i.e., at "resting" membrane potentials). Consistent with this, blocking I_h channels with ZD7288 significantly hyperpolarized the MMP from 56.2 ± 1.4 to 62.5 ± 0.8 mV ($n = 5$; $p < 0.01$) (Fig. 4*A*,*E*,*I*) and increased input resistance (measured at −55 mV) from 245.8 ± 11.4 to 271.2 ± 12.3 MΩ ($p < 0.01$; $n = 5$) (Fig. 3*I*). Thus, I_h contributes ~6 mV to the MMP of ET cells.

What is the role of I_h current in spontaneous bursting? In all five ET cells tested, bursting was terminated by 100 μM ZD7288 (Fig. 4*A–D*,*F–H*). Before the termination of bursting, the frequency decreased [Fig. 4*A* (insets 3 and 4), *B*,*F*] from 2.5 ± 0.4 Hz in control to 0.9 ± 0.2 Hz at 2 min after ZD7288 treatment ($n = 5$; $p < 0.01$), and the duration of the burst envelope increased (Fig. 4*C*,*G*) from 120 ± 3.7 ms in control to 204 ± 23.6 ms at 2 min after ZD7288 treatment ($n = 5$; $p < 0.01$). After its termination, bursting activity was restored (Fig. 4*A–D*,*F–H*) by current injection sufficient to depolarize the membrane potential its original level (Fig. 4*A*,*E*,*I*). However, the current-rescued bursting exhibited a lower frequency (Fig. 4*B*,*F*) at 0.4 ± 0.1 Hz ($n = 5$) and a significant increase in both envelope duration (499 ± 73.2 ms; $n = 5$; $p < 0.001$) and spikes per burst (6.8 ± 1.1; $n = 5$; $p < 0.001$), compared with control, suggesting that I_h also contributes to bursting frequency and burst duration. Together, these results indicate that, in addition to promoting burst generation by repolarizing the membrane potential from its hyperpolarizing level after burst termination, I_h also helps depolarize the membrane potential to a range that facilitates the activation of other conductances, such as I_{NaP}, that are required for burst generation.

ET cells have a prominent low-voltage-activated Ca^{2+} current that is mediated by T- and/or L-type Ca^{2+} channels

Because the rundown experiments indicated a Ca^{2+} dependence of bursting in ET cells, we next investigated the role of voltage-activated Ca^{2+} channels in spontaneous bursting. To isolate Ca^{2+} currents in ET cells, we used Cs^+-methanesulfonate-based intracellular solution containing TEA (20 mM) to block K^+ currents, and added TTX (1 μM) and ZD7288 (100 μM) to the aCSF to eliminate Na^+ and I_h conductances, respectively.

With a holding potential at −70 mV, depolarizing voltage steps (5 mV/step) (Fig. 5*B*) elicited inward currents (Fig. 5*A*) that were abolished by removal of extracellular Ca^{2+} (Fig. 5*B*) with addition of equivalent Mg^{2+} to maintain osmolarity/charge. This Ca^{2+}-dependent current had an activation voltage at approximately −50 mV ($n = 4$) and reached its mean maximum amplitude of 637.0 ± 51.4 pA ($n = 4$) at −30 mV before it decreased with membrane depolarization to 562.8 ± 58.1 pA at −10 mV (Fig. 5*D*, inset). The time-to-peak of this current was voltage dependent (Fig. 5*C*, inset), decreasing from 26.5 ± 3.1 ms at −45 mV to 10.9 ± 0.8 ms at −35 mV ($n = 4$). To better estimate the activation voltage of this current, a conductance–voltage (*G–V*) curve (Fig. 5*D*) was constructed by dividing the current by its driving voltage and fitted with the Boltzmann equation:

$$G(\text{pS}) = [(0.1948 - 3747.6)/(1 + e^{(V+39.73557)})] + 3747.6.$$

Single-channel conductance depends on channel types and even varies for the same type of Ca^{2+} channel from different tissues. For example, with Ca^{2+} as the charge carrier reported single-channel conductance of T-type Ca^{2+} channels and L-type Ca^{2+} channels range ~4–9 pS (Huguenard, 1996; Perez-Reyes, 2003) and ~4–7 pS (Catterall et al., 2005), respectively. For the present purpose, a single-channel conductance of 6 pS was used. The resulting Boltzmann equation gave a Ca^{2+} current an estimated activation threshold voltage of −61 mV. The activation voltage of this LVA Ca^{2+} current is consistent with that of T-type calcium channels, although its inactivation kinetics (Fig. 5*C*), with a time

constant of 61.9 ± 3.2 ms ($n = 4$) for test voltage at −30 mV, is slower than classical T current.

LVA current is generally attributed to the activation of T-type Ca^{2+} channels (Huguenard, 1996). Immunohistochemical and *in situ* hybridization studies indicate that neurons in the olfactory bulb glomerular layer express several T-channel subtypes (Talley et al., 1999; Yunker et al., 2003). Thus, I_{LVA} in ET cells may be mediated, at least in part, by T-channels. To investigate this possibility, we first examined the effect of Ni^{2+}, which blocks T-type calcium channels rapidly and reversibly. I_{LVA} evoked by a 500 ms voltage step from −70 to −30 mV was reversibly blocked by Ni^{2+} in a dose-dependent manner (Fig. 6*C*) with 49.7 ± 3.2% ($n = 5$) blocked at concentrations of 100 μM.

Next, we investigated the role of this Ni^{2+}-sensitive LVA Ca^{2+} current in spontaneous bursting. In 100 μM $NiCl_2$, which blocked ~50% of I_{Ca2+}, spontaneous bursts were terminated but small depolarizing humps persisted (Fig. 6*Ab*). Bursting could be restored by depolarizing current injection (Fig. 6*Ac*). In contrast, 1 mM $NiCl_2$, which blocked >90% of I_{Ca2+} with no effect on I_h and action potential generation (Fig. 6*D*,*E*), reversibly eliminated both spontaneous bursts and depolarizing humps (Fig. 6*Ba–d*). Neither bursting nor the humps were restored by depolarizing current. These results suggest that Ca^{2+} current underlies both the depolarizing envelopes, which generate bursts of action potentials, and the smaller depolarizing humps, which may represent depolarizing envelopes that fail to reach the threshold for action potentials.

Considering the nonselective effect of Ni^{2+} (Tsien et al., 1991; Zamponi et al., 1996), we next investigated the effect of (1*S*,2*S*)-2-(2-(*N*-[(3-benzimidazol- 2-yl) propyl]-*N*-methylamino)ethyl)-6-fluoro-1,2,3,4-tetrahydro-1-isopropyl-2-naphtyl cyclopropanecarboxylate dihydrochloride [NNC 55-0396 (NNC)], a selective T-type calcium channel blocker that does not affect L-type Ca^{2+} channels at concentration up to 100 μM (Huang et al., 2004; Li et al., 2005). Similar to its hydrolysable analog, mibefradil (Bezprozvanny and Tsien, 1995; McDonough and Bean, 1998), the potency of NNC 55-0396 on T-type Ca^{2+} currents (I_T) has a strong voltage dependence (Huang et al., 2004; Li et al., 2005) and increases with membrane depolarization. This was confirmed in the present study. The effect of NNC on Ca^{2+} current elicited by incremental depolarizing voltage steps (5 mV/step) was therefore examined with holding potential at −55 mV, which is the MMP for most ET cells. NNC (50 μM) significantly reduced the LVA calcium current in all ET cells ($n = 4$) at all tested voltages (Fig. 5*G*). At −30 mV NNC (50 μM; 10 min application) inhibited the LVA Ca^{2+} current by 77.7 ± 2.5% ($n = 4$), indicating that most of the LVA current in ET cells was mediated by T-type Ca^{2+} channels (Fig. 5*G*).

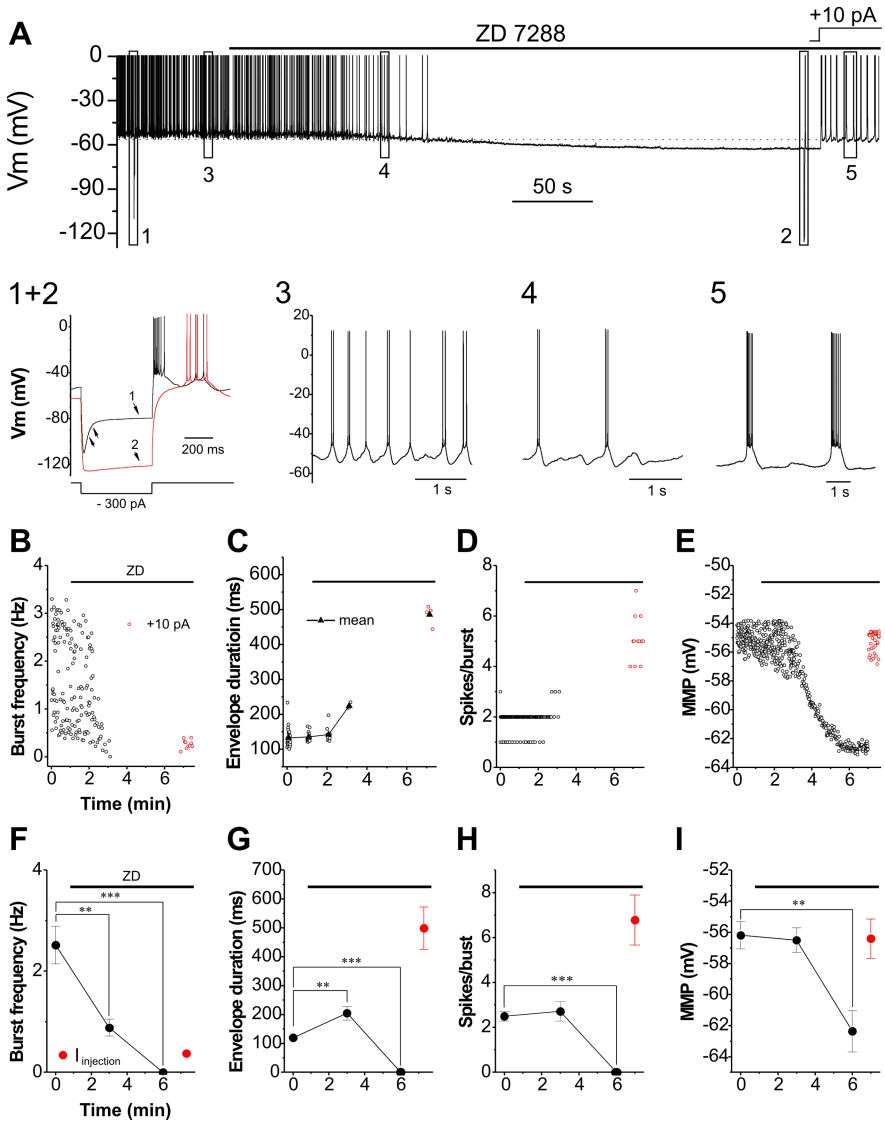

Figure 4. I_h contributes to spontaneous bursting. ***A***, Spontaneous bursting slows (3 and 4) and is eventually terminated by the I_h channel blocker, ZD7288 (100 μM), (top panel). Inset 1 and 2, ZD7288 abolishes the depolarizing sag (arrowheads) and the MMP was hyperpolarized indicating that I_h is active at MMP (see also Fig. 3*G*,*H*). 5, Bursting rescued in the presence of ZD7288 when the MMP restored to original level by depolarizing current injection. ***B–E***, Graphs showing the progressive effects of ZD7288 on burst frequency (***B***), envelope duration (***C***), spikes per burst (***D***), and MMP (***E***) of cell in ***A***. ***F–I***, Average changes for five cells. Error bars indicate SEM. $^{**}p < 0.01$; $^{***}p < 0.001$.

Window T-type Ca^{2+} current-mediated bistability underlies the expression of the slow oscillatory or rhythmic activity as well as high-frequency bursting firing in some neurons (Crunelli et al., 2005). However, the mean half-activation and half-steady-state inactivation voltages of the LVA Ca^{2+} were −37.1 and −59.2 mV ($n = 5$), respectively. This gave an estimated window current in ET cells at MMP (approximately −55 mV) of 3.8 ± 2.9 pA (Fig. 5*F*), indicating little estimated contribution (~0.9 mV) to the MMP. Thus, the LVA Ca^{2+} window current plays no obvious role in ET cell bursting.

The glomerular layer also shows immunoreactivity to L-type Ca^{2+} channels (Grunnet and Kaufmann, 2004), some of which also have low activation voltages (Lipscombe et al., 2004). Murphy et al. (2005) reported that L-type Ca^{2+} channels mediate LVA I_{Ca} in PG cells. Thus, we investigated the effect of nimodip-

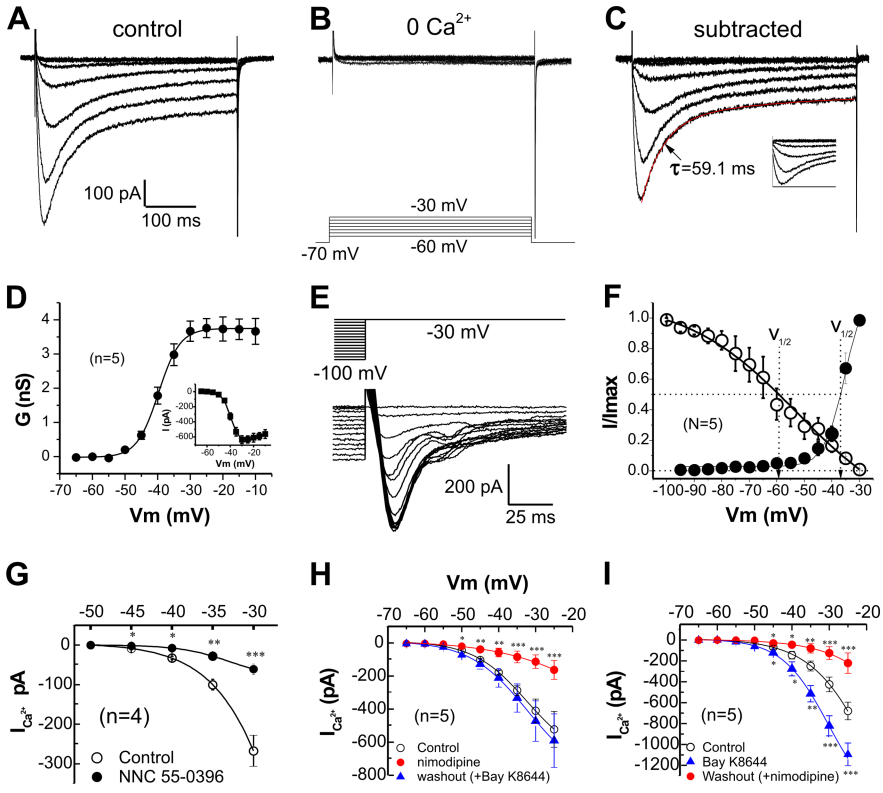

Figure 5. ET cells have a prominent LVA Ca^{2+} current mediated by L- and/or T-type Ca^{2+} channels. ***A***, Inward currents generated by depolarizing voltage steps with membrane potential held at −70 mV in aCSF containing TTX (1 μM) and ZD7288 (100 μM). ***B***, Same cell with aCSF containing 0 mM Ca^{2+}/2.6 mM Mg^{2+} and 0.3 mM EGTA. ***C***, ***A*** minus ***B*** shows Ca^{2+} current. ***D***, *G–V* curve of the peak Ca^{2+} current from five cells fitted with Boltzmann equation. Inset, The corresponding *I–V* curve. ***E***, Steady-state inactivation of Ca^{2+} current. A −30 mV test pulse was preceded by incremental (5 mV/step) hyperpolarizing pulses (10 s) from −100 mV. ***F***, Activation ($V_{1/2} = -37.1$ mV) and inactivation ($V_{1/2} = -59.2$ mV) *I–V* curves of five cells expressed as a function of membrane voltage and fitted with Boltzmann equations shows very little Ca^{2+} current at MMP. ***G***, *I–V* curves of peak Ca^{2+} currents with holding potential at −55 mV showing that NNC 55-0396 (50 μM), a selective T-type Ca^{2+} channel blocker, significantly reduces I_{Ca2+} ($n = 4$ cells). ***H***, *I–V* curves of the peak Ca^{2+} current showing that nimodipine (20 μM), an L-type Ca^{2+} channel blocker, significantly reduces I_{Ca2+}. After nimodipine washout with addition of Bay K8644 (5 μM), an L-type Ca^{2+} channel activator, I_{Ca2+} is restored ($n = 5$ cells). ***I***, *I–V* curves of the peak Ca^{2+} current showing that Bay K8644 (5 μM) increases I_{Ca2+}, and its activation voltage shifts from −50 to −55 mV. After Bay K8644 washout, addition of nimodipine (20 μM) reduces I_{Ca2+} ($n = 5$ cells). Error bars indicate SEM. $^*p < 0.05$; $^{**}p < 0.01$; $^{***}p < 0.001$ compared with control.

ine, an L-type Ca^{2+} channel blocker on ET cells. At 20 μM, nimodipine reduced I_{Ca2+} at all voltages tested (Fig. 5*H*). Nimodipine reduced peak Ca^{2+} current from 45.1 ± 2.5 to 19.3 ± 6.9 pA ($n = 5$; $p < 0.05$) at −50 mV and from 409.6 ± 7.3 to 113.1 ± 42.3 pA ($n = 5$; $p < 0.01$) at −30 mV, respectively. This reduction was reversed on nimodipine washout and addition of 1,4-dihydro-2,6-dimethyl-5-nitro-4[trifluoromethyl-phenyl]-3-pyridinecarboxylic acid methylester [Bay K8644 (BayK)], an L-type Ca^{2+} channel activator (Fig. 5*H*). Ten minutes after BayK (5 μM) application, I_{Ca2+} increased from 19.3 ± 6.9 to 72.6 ± 13.3 pA ($n = 5$; $p < 0.01$) at −50 mV and from 113.1 ± 42.3 to 472.2 ± 122.4 pA ($n = 5$; $p < 0.05$) at −30 mV. In separate experiments, slices were treated first with BayK followed by washout of BayK plus addition of nimodipine (Fig. 5*I*). BayK (5 μM; 5 min) increased peak Ca^{2+} current from 35.6 ± 12.4 to 62.2 ± 19.9 pA ($n = 5$; $p < 0.05$) at −50 mV and from 425.1 ± 70.2 to 821.4 ± 96.2 pA ($n = 5$; $p < 0.01$) at −30 mV, respectively. When BayK was replaced with nimodipine (20 μM), I_{Ca2+} was reduced from 62.2 ± 19.9 to 9.3 ± 2.4 pA ($n = 5$; $p < 0.05$) at −50 mV and from 821.4 ± 96.2 to 125.5 ± 61.6 pA at −30 mV ($n = 5$; $p < 0.01$).

R-type calcium currents contribute to bursting in hippocampal neurons (Metz et al., 2005) and are also sensitive to low concentrations of Ni^{2+}. However, LVA Ca^{2+} currents in ET cells were insensitive to SNX-482 (400 nM), a selective R-type calcium channel blocker (Bourinet et al., 2001) (data not shown) (mean peak I_{Ca} in five cells changing from 585.5 ± 49.0 pA in control to 559.7 ± 42.0 pA after SNX-482 measured at −30 mV with holding potential at −70 mV), indicating no involvement of SNX-482-sensitive R-type channels.

In summary, ET cells have an LVA Ca^{2+} current that is mediated by T- and/or L-type Ca^{2+} channels. Its sensitivity to NNC 55-0396 and its relatively low activation voltage suggest that the isolated LVA Ca^{2+} current is mediated by T-type Ca^{2+} channels. However, unlike classical T-type Ca^{2+} currents, the ET cell LVA Ca^{2+} current exhibited slow inactivation kinetics ($\tau = \sim 62$ ms for test voltage at −30 mV). This could be attributable to $Ca_V3.3$ ($\alpha 1I$) T-type channels, which exhibit slow inactivation kinetics (Park et al., 2004) and relatively low sensitivity of Ni^{2+} (Zamponi et al., 1996). $Ca_V3.3$ mRNA and protein are expressed at high levels in olfactory bulb glomeruli (Talley et al., 1999; Yunker et al., 2003).

The contribution of L-type Ca^{2+} channels to the LVA current in ET cells is supported by its slow inactivation and its sensitivity to the dihydropyridine agonist, Bay K8644 and the antagonist, nimodipine. L-type channels have traditionally been regarded as high-voltage-activated (HVA) Ca^{2+} channels, although, dihydropyridine-sensitive LVA Ca^{2+} currents have been reported in a number of neurons, including rat olfactory bulb PG cells (Avery and Johnston, 1996; Magee et al., 1996; Murphy et al., 2005). Of the four L-type channels (Cav1.1/α_{1S}, Cav1.2/α_{1C}, Cav1.3/α_{1D}, and Cav1.4/α_{1F}), Cav1.3/α_{1D} expresses ubiquitously in the mammalian brain including the bulb (Hell et al., 1993; Ludwig et al., 1997) and activates at relatively low membrane potentials (approximately −55 mV) (Koschak et al., 2001; Xu and Lipscombe, 2001; Lipscombe et al., 2004). In addition, channels containing Cav1.3/α_{1D} have a relatively lower sensitivity to dihydropyridine antagonists, including nimodipine. The ET cell LVA Ca^{2+} current was partially blocked by 20 μM but not 10 μM nimodipine. This may be because most of the current is mediated by T-type channels and/or because it is partly mediated by Cav1.3 L-type channels. Involvement of L-type channels in the ET cell LVA current would also account for its slow kinetics because all L-type channels inactivate slowly (Catterall et al., 2005).

Activation of T-type Ca^{2+} channels is required for low-threshold Ca^{2+} spikes and spontaneous bursting

In agreement with the voltage-clamp experiments, low-threshold Ca^{2+} spikes (LTSs) were evoked by current pulses in current clamp with holding potential at −62 to −65 mV in the presence of TTX (Figs. 7*A*, 8*A*, 9*A*). The activation threshold for these

all-or-none LTSs was −46.9 ± 0.7 mV ($n = 15$). NNC 55-0396 (50 μM) (Fig. 7*B*) abolished LTSs in all five cells, indicating the requirement of T-type Ca^{2+} current.

LTSs have been implicated in pacemaker function because an LTS typically triggers a burst of action potentials (Huguenard, 1996; Perez-Reyes, 2003). To investigate the role of the T-type calcium channel-mediated LTS in spontaneous bursting, we tested the effect of NNC 55-0396 (50 μM; 10 min) on ET cells recorded in current clamp. NNC irreversibly abolished spontaneous bursting with no effect on MMP (Fig. 7*C*,*G*,*K*). Bursting could not be restored either by depolarizing or hyperpolarizing current injection (Fig. 7*C*). NNC did not alter the ability of the cells to fire action potentials (Fig. 7*C*, blowup). Before termination of bursting, burst frequency (Fig. 7*C*,*D*,*H*), envelope duration (Fig. 7*E*,*I*), and spikes per burst (Fig. 7*F*,*J*) all decreased with time in NNC. Measured 6 min after NNC 55-0396 treatment, burst frequency decreased from 2.7 ± 0.6 to 0.6 ± 0.2 Hz ($n = 5$; $p < 0.01$), envelope duration from 111.1 ± 9.2 to 64.3 ± 6.0 ms ($n = 5$; $p < 0.01$), and spikes per burst from 3.4 ± 0.3 to 1.8 ± 0.1 ($n = 5$; $p < 0.01$). These results support an essential role of T-type calcium channels in spontaneous ET cell burst generation.

L-type Ca^{2+} channels are required for LTSs and modulate spontaneous bursting

Because the voltage-clamp experiments also provided evidence for the involvement of L-type Ca^{2+} channels in LVA I_{Ca}, we next investigated their role in LTSs. After exposure to nimodipine (20 μM; 10 min), LTSs were abolished in all five ET cells tested (Fig. 8*B*). This was partially reversed after replacement of nimodipine with Bay K8644 (5 μM; 15 min) (Fig. 8*C*). In separate experiments, LTSs were significantly prolonged in duration by BayK (5 μM) (Fig. 9*A*,*B*); LTS duration measured at −40 mV increased from 112.4 ± 6.7 to 205.9 ± 8.7 ms ($n = 5$; $p < 0.01$). The prolongation of LTSs was reversed by washout of BayK with addition of nimodipine (20 μM) (Fig. 9*C*). These results support the involvement of L-type Ca^{2+} channels in LTSs.

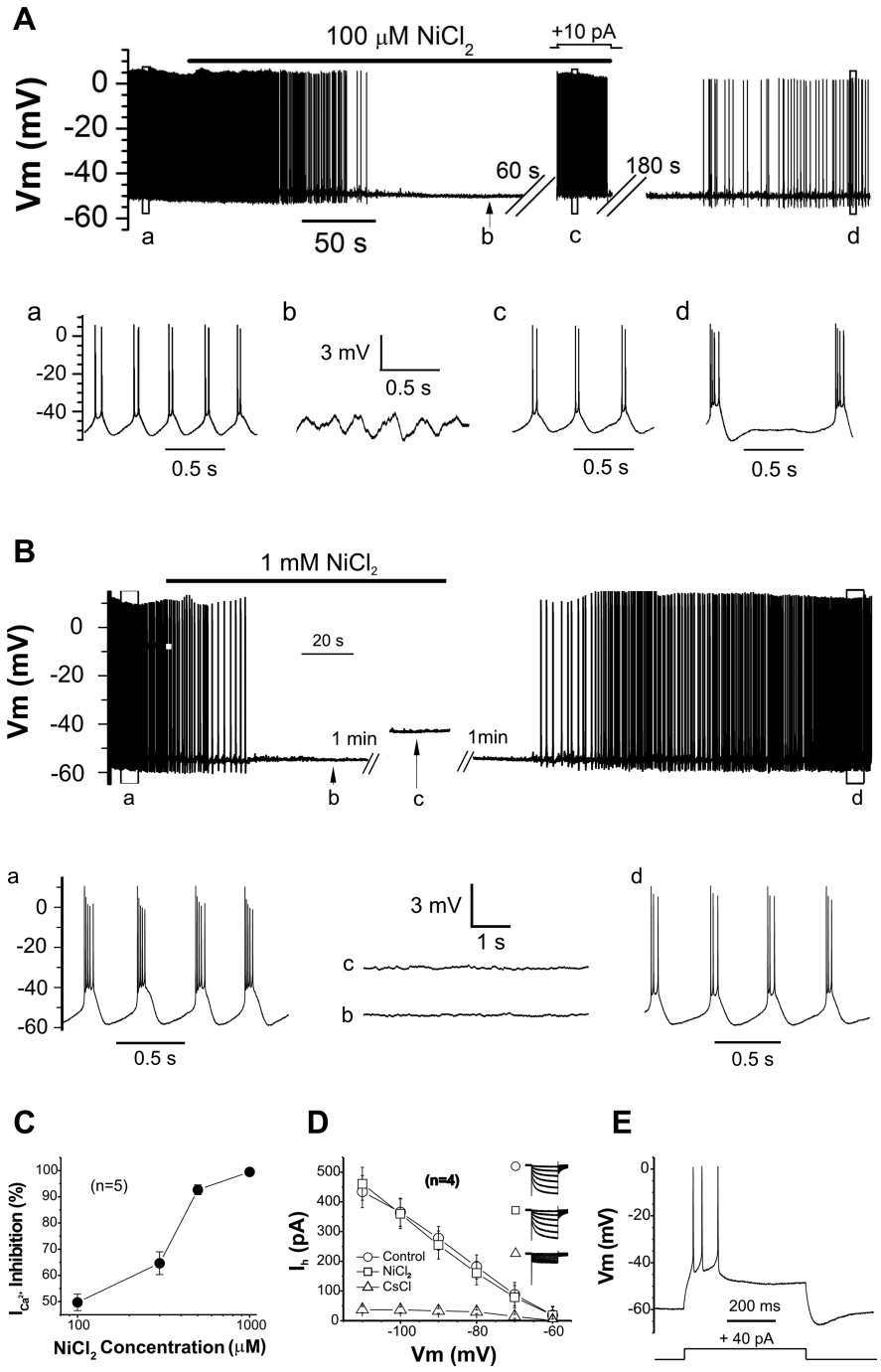

Figure 6. Effect of Ni^{2+} on spontaneous bursting. ***A***, Bath application of 100 μM $NiCl_2$ reversibly terminates the spontaneous bursting, which can be restored by 10 pA depolarizing steady current injection to bring the membrane potential to its original level (expanded trace ***c***). Spontaneous voltage humps (expanded trace ***b***) persist. ***B***, Bath application of 1 mM $NiCl_2$ reversibly terminates spontaneous bursting, which cannot be restored by depolarizing steady current injection. Note that there are no spontaneous or evoked voltage humps in the presence of 1 mM $NiCl_2$ (expanded traces ***b*** and ***c***). ***C***, Dose–response curve from five cells showing the inhibitory effect of $NiCl_2$ on Ca^{2+} currents evoked by voltage step to −30 mV with holding potential at −70 mV. ***D***, *I–V* curve from four cells showing that I_h is blocked by 2 mM CsCl but not affected by 1 mM $NiCl_2$ at all tested voltages when membrane was held at −55 mV. Error bars indicate SEM. ***E***, Action potentials are evoked by a depolarizing current step in the presence of 1 mM $NiCl_2$.

We next investigated the role of L-type channels in spontaneous bursting. Nimodipine (20 μM) decreased both envelope duration [Fig. 8*D* (blowups), *F*,*J*] and spikes per burst [Fig. 8*D* (blowups),*G*,*K*]. The mean envelope duration (Fig. 8*J*) and spikes per burst (Fig. 8*K*) in five cells decreased from 105.1 ± 13.6 to 76.0 ± 9.4 ms ($n = 5$; $p < 0.05$) and 2.4 ± 0.1 to 1.0 ± 0.01 ($n = 5$; $p < 0.01$), respectively. Although nimodipine did not eliminate bursting, the attenuated depolarizing envelopes generated only single spikes (Fig. 8*D*,*G*,*K*). If we count envelopes with only single spikes as "bursts," burst frequency was not significantly affected by nimodipine (Fig. 8*E*,*I*). Nimodipine also depolarized the membrane potential (Fig. 8*D*,*H*,*L*) from −57.1 ± 1.2 to −54.0 ± 1.2 mV ($n = 5$; $p < 0.01$). Restoring the MMP to its original level by hyperpolarizing current

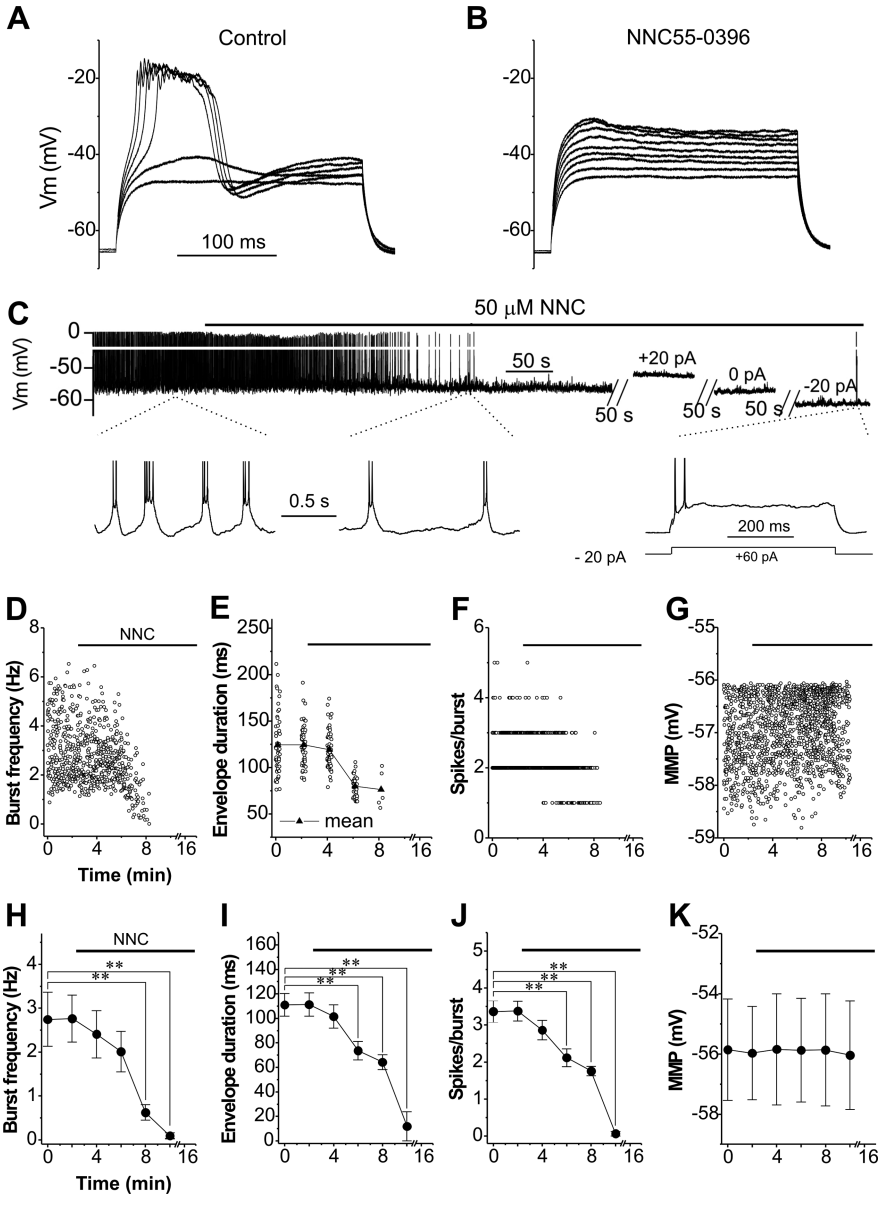

Figure 7. Blocking T-type Ca^{2+} channel eliminates LTSs and terminates spontaneous bursting. ***A***, All-or-none Ca^{2+} spikes were evoked by intracellular current injection in the presence of TTX (1 μM). ***B***, Blocking T-type Ca^{2+} channels with NNC 55-0396 (50 μM) abolishes LTSs. ***C***, Current-clamp recording (no TTX) showing that NNC 55-0396 (50 μM) slows and then terminates spontaneous bursting. Bursting is not restored by either positive or negative current injection, but action potentials are elicited by positive current injection in the presence of NNC. ***D–G***, Graphs showing the effect of NNC 55-0396 on burst frequency (***D***), envelope duration (***E***), spikes per burst (***F***), and MMP (***G***) of the cell in ***C***. ***H–K***, Averaged data ($n = 5$ cells) showing the effect of NNC 55-0396 on the same burst parameters. Error bars indicate SEM. $^{**}p < 0.01$.

injection increased envelope duration, but did not increase spikes per burst, indicating that those changes were not entirely attributable to nimodipine-induced membrane depolarization.

All changes in bursting were reversed after replacing nimodipine with Bay K8644 (5 μM; 12 min) (Fig. 8*D*,*F–H*,*J–L*). Specifically, envelope duration (Fig. 8*J*), spikes per burst (Fig. 8*K*), and MMP (Fig. 8*L*) changed from 76.0 ± 9.4 to 126.6 ± 7.7 ms ($n = 5$; $p < 0.05$), 1.0 ± 0.01 to 2.5 ± 0.1 ($n = 5$; $p < 0.01$), and −54.0 ± 1.2 to 56.9 ± 1.4 mV ($n = 5$; $p < 0.01$), respectively. In separate experiments, BayK was applied first, and then nimodipine was added during washout. In this condition (Fig. 9*D*), BayK (5 μM) increased envelope duration (Fig. 9*F*,*J*) and spikes per burst (Fig. 9*G*,*K*) over control values from 89.4 ± 10.7 to 160.8 ± 19.5 ms ($n = 5$; $p < 0.05$) and 2.8 ± 0.2 to 6.6 ± 0.5 ($n = 5$; $p < 0.01$), respectively. The MMP was hyperpolarized from −55.3 ± 1.4 to −59.3 ± 3.7 mV (Fig. 9*H*,*L*) with little effect on burst frequency (Fig. 9*E*,*I*). Washout of BayK plus addition of 20 μM nimodipine (Fig. 9*D*,*F–H*,*J–L*) reversed all effects of BayK except burst frequency, which was reduced from 3.2 ± 0.1 to 1.3 ± 0.2 Hz ($n = 5$; $p < 0.01$). However, neither envelope duration nor spikes per burst was reversed by restoring MMP to its original level with depolarizing current (Fig. 9*D*,*F*,*G*,*J*,*K*), suggesting that the effect of BayK on bursting was not attributable to a change of membrane potential. Together, these results support the idea that L-type Ca^{2+} channels prolong the duration of the depolarizing envelope and increase the number of spikes per burst.

A large-conductance Ca^{2+}-dependent K^+ (BK) current regulates burst duration

The results to this point show that two inward conductances, I_{NaP} and I_h, contribute to the initiation of bursting by depolarizing the membrane potential to the threshold for LVA Ca^{2+} spikes, which comprise the depolarizing envelope on which a burst of action potentials is generated. What terminates the burst? Burst termination requires a mechanism that hyperpolarizes the membrane potential sufficiently to turn off the inward conductances that support the depolarizing envelope. Conceivably, passive inactivation of inward conductances (I_{NaP}, $I_{T/L}$, or both), engagement of outward conductances that deactivate the inward currents, or a combination of both factors could provide this mechanism. Lacking selective pharmacological tools to manipulate the inactivation of I_{NaP} or $I_{T/L}$, we investigated the possibility that outward conductance regulate the burst duration.

$I_{T/L}$, which is active throughout the depolarizing envelope, elevates cytosolic calcium that can trigger or modulate intracellular targets, including activation of Ca^{2+}-dependent ion channels. Ca^{2+}-activated potassium channels (K_{Ca2+}) are broadly divided into three subtypes based on their biophysical and pharmacological profiles: small- (SK), intermediate- (IK), and large-conductance (BK) channels. Although activation of any of these three can cause membrane hyperpolarization, the following considerations make BK an attractive candidate for terminating bursting in ET cells: (1) there is strong BK immunoreactivity in the glomerular layer (GL) of mouse olfactory bulb (Sausbier et al., 2006); (2) activation of BK channels is both voltage and Ca^{2+} dependent, so that deactivation of this outward conductance can be very rapid and complete on membrane hyperpolarization; and (3) BK chan-

nels have large conductance so that their activation can produce strong membrane hyperpolarization.

We first asked whether ET cells have functional BK channels. To record maximal BK currents, a 300 ms hyperpolarizing (−100 mV) prepulse (to de-inactivate both BK channels and voltage-dependent calcium channels) was applied before incremental depolarizing voltage steps (500 ms; 5 mV/step) from −70 to −15 mV with holding potential at −70 mV (Fig. 10*B*, inset). With TTX and ZD7288 in the bath to block Na^+ and I_h currents, this protocol revealed an outward current (Fig. 10*A*) that activated at −42.0 ± 1.2 mV ($n = 5$) and increased with membrane depolarization from 44.3 ± 9.5 pA at −35 mV to 573.9 ± 13.6 pA ($n = 5$) at −15 mV.

The BK channel selective blocker, IBTX (200 nM; 15 min), significantly reduced (Fig. 10*B*) this voltage-dependent outward current from 44.3 ± 9.5 to 19.8 ± 6.8 pA ($n = 5$; $p < 0.05$) at −35 mV, and from 573.9 ± 13.6 to 197.4 ± 78.3 pA ($n = 5$; $p < 0.01$) at −15 mV. The IBTX-sensitive outward current (Fig. 10*C*, inset) activated at about −39.0 ± 1.0 mV and increased in amplitude with membrane depolarization (Fig. 10*C*) ($n = 5$) from 24.5 ± 4.8 pA at −35 mV to 375.9 ± 118.4 pA at −15 mV, indicating that ET cells have functional BK channels. The residual IBTX-resistant outward currents may reflect incomplete block of BK by IBTX or the involvement of other potassium channels.

Next, we investigated the role of this current in bursting. In current clamp and with the membrane potential held around −70 mV by steady current injection to prevent spontaneous bursting, 400 ms depolarizing current pulses were applied to evoke a single burst per pulse (Fig. 10*D*); 10 evoked bursts were collected at 0.2 Hz from each ET cell and compared with 10 bursts evoked in the presence of IBTX (200 nM; 15 min treatment). As shown in Figure 10*D*, IBTX treatment significantly increased the duration of evoked bursts by 45.5% from 112.8 ± 4.7 to 163.5 ± 6.2 ms ($n = 4$ cells; $p < 0.01$) without affecting input resistance measured at −55 mV (from 227.5 ± 10.3 MΩ in control to 240.6 ± 12.8 MΩ at 15 min after IBTX; $n = 4$ cells).

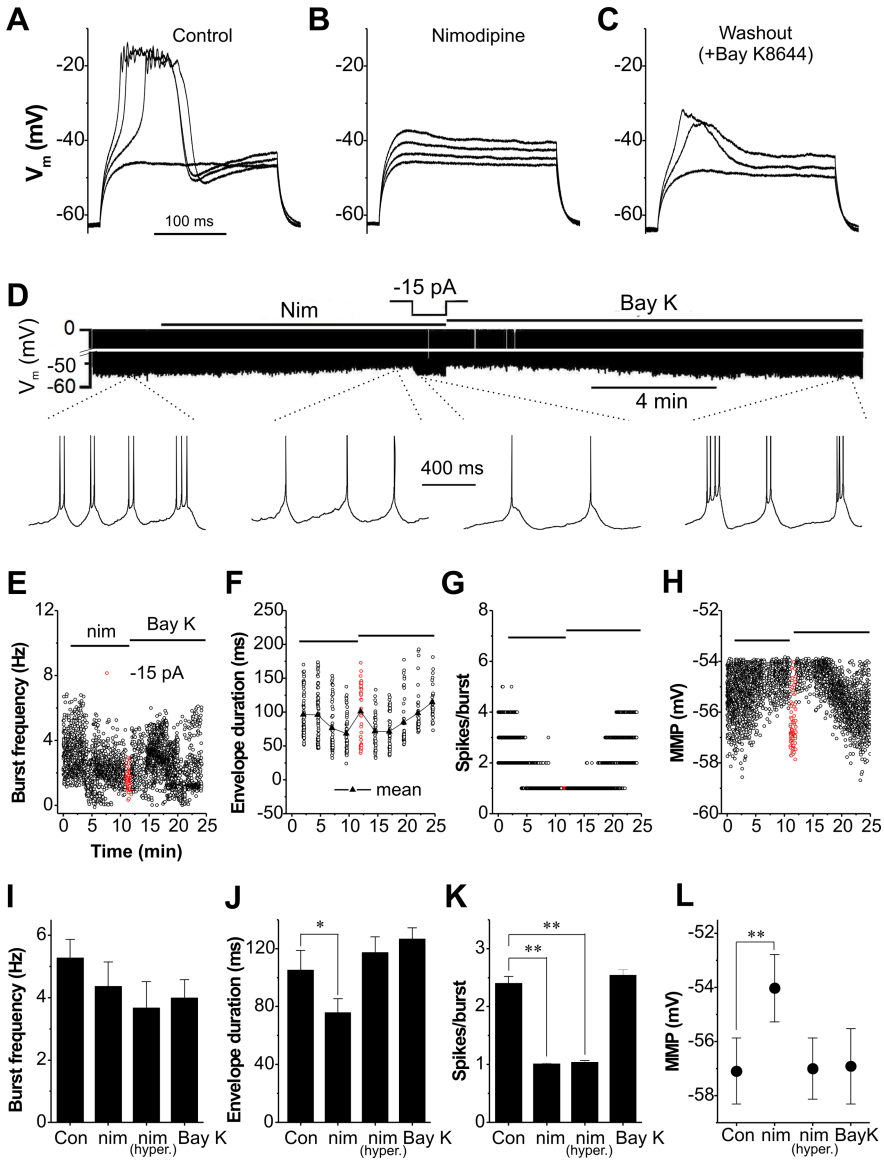

Figure 8. Blocking L-type channels eliminates evoked LTSs and reduces number of spikes per spontaneous burst. ***A***, All-or-none calcium spikes evoked by intracellular current injection in the presence of TTX (1 μM). ***B***, Blocking L-type Ca^{2+} channels with nimodipine (20 μM) abolishes LTSs. ***C***, Washout of nimodipine with addition of Bay K8644 (5 μM) partially rescues LTSs. ***D***, Current-clamp recording of spontaneous bursting (no TTX) showing that nimodipine (20 μM) reduces both envelope duration and spikes per burst. Effect on spikes per burst is not attributable to membrane depolarization because it was not reversed by injection of steady hyperpolarization current to restore the MMP to pre-nimodipine levels. Addition of BayK (5 μM) during nimodipine washout rescues bursting (traces below expanded timescale). ***E–H***, Graphs showing effect of nimodipine and washout of nimodipine plus BayK on burst frequency (***E***), envelope duration (***F***), spikes per burst (***G***), and MMP (***H***) of cell in ***D***. ***I–L***, Mean burst frequency (***I***), envelope duration (***J***), spikes per burst (***K***), and MMP (***L***) ($n = 5$ cells) immediately before (con), 9 min after nimodipine (nim), nimodipine with hyperpolarizing current injection (nim + hyper), and 12 min after washout of nimodipine plus BayK (Bay K). Averages were measured for 20 s for each condition for each cell. Error bars indicate SEM. *$p < 0.05$; **$p < 0.01$.

What activates I_{BK}? Because $I_{L/T}$ plays an important role in spontaneous bursting (Figs. 5–9), $I_{L/T}$ might conceivably provide both depolarization and intracellular Ca^{2+} $[Ca^{2+}]_i$ elevation for BK channel activation. Although our voltage-clamp data already indicated that very little I_{BK} is activate at membrane potentials more negative than −30 mV (Fig. 10*C*) and because the depolarizing envelopes never exceed −40 mV, BK channel activation might conceivably be shifted to a more negative voltage range by $[Ca^{2+}]_i$ elevation through $I_{T/L}$. If this were the case, BK channels should play a role in terminating LTSs. Alternatively, $I_{T/L}$ may be insufficient to increase $[Ca^{2+}]_i$ for BK channel activation within the voltage range of the depolarizing envelope. In this scenario, transient sodium channel (I_{NaT})-mediated action potentials rather than the $I_{L/T}$-mediated LTSs might be required to activate BK channels because, in addition to strong depolarization, action potentials can also increase $[Ca^{2+}]_i$ by activating HVA Ca^{2+} channels (I_{HVA}).

To test the first hypothesis, we examined the effect of IBTX on evoked LTSs in the presence of TTX (1 μM) and ZD7288 (100

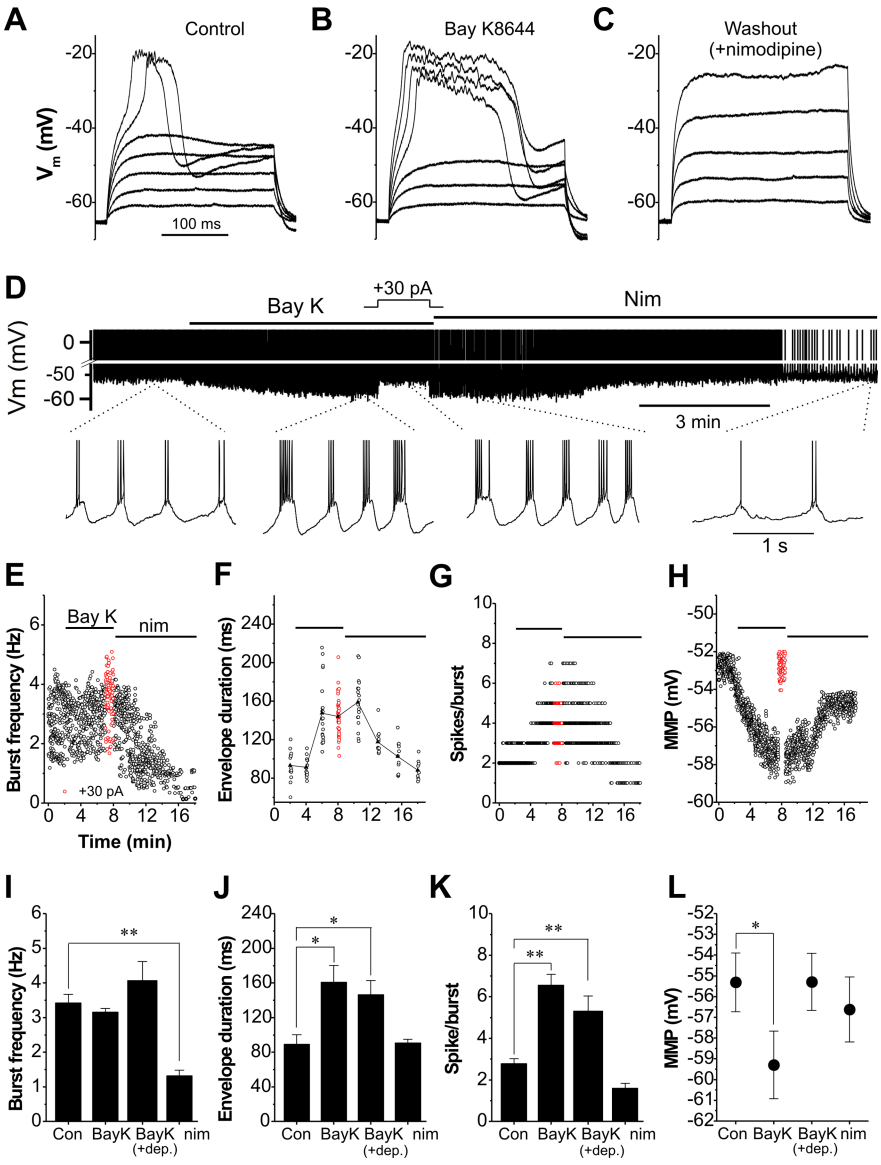

Figure 9. Activation of L-type Ca^{2+} channels prolongs evoked LTSs and spontaneous bursts. ***A***, All-or-none calcium spikes evoked by intracellular current injection in the presence of TTX. ***B***, Bay K8644 5 (μM) increases LTS duration and reduces LTS activation threshold from 44.5 ± 1.7 to −48.5 ± 1.5 mV ($n = 5$; $p < 0.01$). ***C***, BayK washout with addition of nimodipine (20 μM) abolishes LTSs. ***D***, In spontaneous bursting (no TTX), BayK (5 μM) increases both burst duration and spikes per burst without changing burst frequency. Effects are not attributable to BayK-induced membrane hyperpolarization because they persist during depolarizing current injection that restores MMP to pre-BayK baseline. Washout of BayK plus nimodipine (20 μM) restores bursting to control values (expanded traces below). ***E–H***, Graphs showing the progressive effects of BayK, BayK plus 30 pA depolarizing current, and BayK washout plus nimodipine on the burst frequency (***E***), envelope duration (***F***), spikes per burst (***G***), and MMP (***H***) of the cell in ***D***. ***I–L***, Mean burst frequency (***I***), envelope duration (***J***), spikes per burst (***K***), and MMP (***L***) from five cells in control (con) and 4 min after BayK, BayK plus depolarization (BayK+dep), and 10 min after washout of BayK plus nimodipine (nim), respectively. Error bars indicate SEM. *$p < 0.05$; **$p < 0.01$.

μM) to block action potentials and I_h and found that blocking BK channels with IBTX (200 nM; 15 min) did not change LTS duration (control, 90.8 ± 7.3 ms; IBTX, 91.4 ± 8.5 ms; $n = 5$) (Fig. 10*E*). Therefore, the depolarizing voltage and Ca^{2+} associated with $I_{T/L}$ are insufficient to activate I_{BK}. Thus, the depolarizing envelope, by itself, is unlikely to engage this conductance.

We next explored the contribution of I_{HVA} to BK channel activation and the duration of evoked bursts by blocking I_{HVA} with ω-conotoxin MVIIC, which at high concentration blocks both P/Q- and N-type Ca^{2+} channels (McDonough et al., 1996). As shown in Figure 10*F*, ω-conotoxin MVIIC (5 μM; 10 min) increased evoked burst duration by 31.7% from 93.7 ± 6.4 to 123.4 ± 2.5 ms ($n = 5$; $p < 0.01$). There was no effect on input resistance measured at −55 mV (control, 231.1 ± 19.4 MΩ; conotoxin MVIIC, 236.3 ± 11.2 MΩ; $n = 5$). The smaller increase in the depolarizing envelope duration by conotoxin MVIIC (31.7%) compared with IBTX (45.5%) may reflect an incomplete block of HVA Ca^{2+} current by conotoxin MVIIC or the possibility that a strong membrane depolarization during action potentials and LVA Ca^{2+} current combine to activate BK channels. This finding indicates that I_{HVA} is required for BK channel activation and supports the hypothesis that BK channels are activated by both $[Ca^{2+}]_i$ increase and strong depolarization during action potentials.

In addition to increasing depolarizing envelope duration, treatment with IBTX or conotoxin MVIIC also reduced the decay slope of action potentials within bursts. As shown in Figure 10, *G–I*, IBTX (200 nM; 15 min) decreased the decay slope by 29.7% from 74.8 ± 8.2 to 52.6 ± 7.7 mV/ms ($n = 5$; $p < 0.05$) for the first action potential, by 37.3% from 53.6 ± 4.3 to 33.6 ± 6.0 mV/ms ($n = 5$; $p < 0.01$) for the second one, by 38.3% from 47.8 ± 5.4 to 29.5 ± 3.6 mV/ms for the third one within each burst, respectively. Conotoxin MVIIC (5 μM; 10 min) reduced the decay slope by 18.8% from 72.3 ± 2.7 to 58.7 ± 1.8 mV/ms for the first action potential, by 34.2% from 51.0 ± 1.7 to 33.6 ± 4.2 mV/ms for the second one, and by 40.3% from 43.2 ± 3.0 to 25.8 ± 2.5 mV/ms for the third one within each burst, respectively. These results indicate a contribution of BK and HVA Ca^{2+} currents to the repolarization of action potentials.

Finally, we investigated the role of I_{BK} in spontaneous bursting. As shown in Figure 11*A*, IBTX increased both envelope duration (Fig. 11*C*,*G*) and spikes per burst (Fig. 11*D*,*H*) without significantly affecting either burst frequency (Fig. 11*B*,*F*) or MMP (Fig. 11*E*,*I*). The average envelope duration (Fig. 11*G*) from five cells increased by 57.5% from 106.8 ± 16.5 to 167.1 ± 31.1 ms ($n = 5$; $p < 0.05$) and spikes per burst (Fig. 11*H*) increased from 3.0 ± 0.2 to 4.8 ± 0.2 ($n = 5$; $p < 0.01$). Together, these results support the hypothesis that BK current regulates burst duration by contributing to burst termination.

SK channel immunostaining has also been detected in the mouse glomerular layer (Sailer et al., 2004). This type of K_{Ca} channel plays a role in dendrodendritic inhibition in the olfactory bulb by regulating dendritic excitability of mitral cells (Maher and Westbrook, 2005). Therefore, we tested the role of SK in ET cell bursting with both apamin (300 nM), a selective blocker of SK channels, and bicuculline (30 μM), a $GABA_A$ receptor blocker that also blocks both apamin-sensitive and apamin-insensitive

SK channels (Khawaled et al., 1999). Because bicuculline was applied at least 10 min after gabazine (10 μM), a specific $GABA_A$ receptor blocker, any effect on bursting should attribute to SK channels. As shown in Figure 11, *F–I*, none of the bursting parameters measured was significantly affected, indicating that SK channels do not play an obvious role in the regulation of spontaneous bursting of ET cells.

Discussion

ET cells in mouse olfactory bulb fire spontaneous bursts of action potentials in the absence of fast synaptic inputs. The present study demonstrates that this ability to generate autonomous bursts depends on multiple, voltage-dependent ionic conductances, including I_h, I_{NaP}, I_T and/or I_L, I_{HVA}, and I_{BK}. These intrinsic conductances are precisely orchestrated to produce rhythmical spontaneous bursting in mouse ET cells.

I_h regulates minimum membrane potential and is required for spontaneous bursting

I_h plays a key role in setting the MMP in ET cells. It begins to activate at approximately −45 mV, which is 10 mV positive to the MMP (approximately −55 mV) suggesting that I_h generates significant steady-state inward current at both average and minimum membrane potentials. Consistent with this, ZD7288 produced a significant hyperpolarization and increased input resistance (R_{in}). Because I_h does not inactivate (Luthi and McCormick, 1998), it operates like an inward "leak" current around MMP, counterbalancing active outward currents that could further hyperpolarize the membrane. When I_h was blocked by ZD7288, spontaneous bursting was eliminated, but was restored by current sufficient to bring the hyperpolarized MMP back to control levels. Therefore, I_h functions to limit postburst hyperpolarization and depolarizes the membrane to the activation voltages of other conductances (I_{NaP} and $I_{T/L}$) required for burst generation.

Na^+ dependence of ET cell spontaneous bursting

The observation that repetitive bursting was restored by depolarizing current in the presence of ZD7288 indicated that additional voltage-dependent inward currents are required for burst generation. These conductances must be active near the MMP (approximately −55 mV). One such current is I_{NaP} (Crill, 1996), which has been proposed to drive pacemaker activity in many neurons. Consistent with our previous study in rats (Hayar et al., 2004a), mouse ET cells have a TTX-sensitive I_{NaP}, which activates at approximately −60 mV, ~5 mV negative to MMP. I_{NaP} increases with membrane depolarization, depolarizes the membrane to the activation threshold of $I_{T/L}$, and is active throughout the voltage range of the burst envelope. Spontaneous bursting is abolished by TTX and cannot be restored by current injection. Thus, I_{NaP} is essential for burst generation in mouse ET cells.

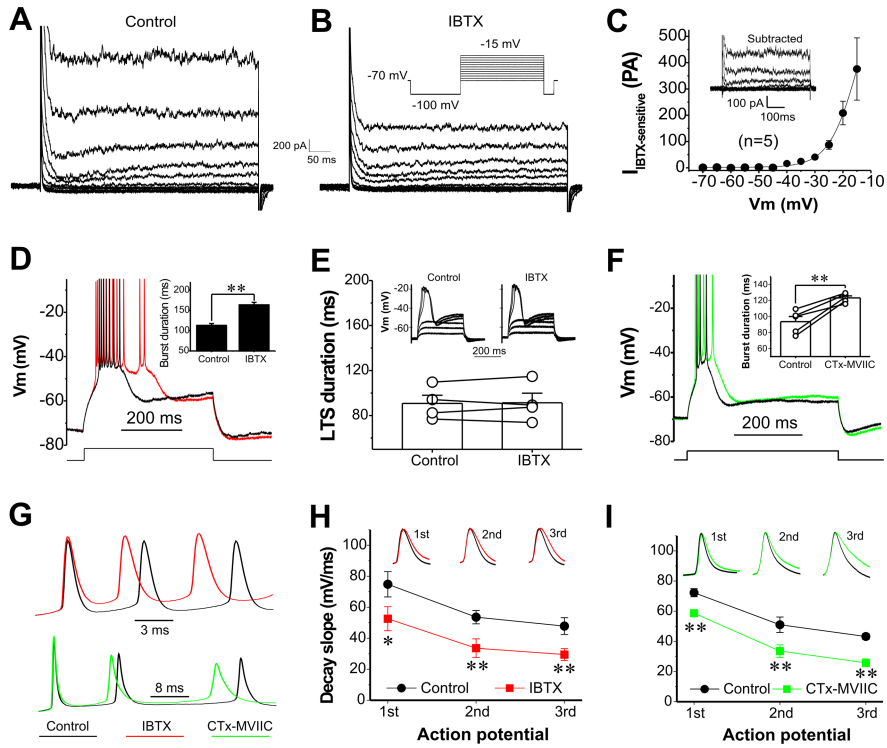

Figure 10. Large-conductance Ca^{2+}-dependent potassium (BK) current regulates evoked burst termination. ***A***, ***B***, Voltage-clamp recording using the protocol shown in ***B*** (inset) in aCSF containing TTX (1 μM) with (***B***) or without (***A***) IBTX (200 nM), a selective BK channel blocker, to identify BK currents. ***C***, Averaged *I–V* curve of IBTX-sensitive currents from five cells. Inset, Subtracted traces (***A*** minus ***B***) showing the IBTX-sensitive currents. ***D***, Current-clamp recordings comparing burst duration before (black) and after (red) IBTX (200 nM), showing that burst duration is significantly lengthened by blocking BK channels. Inset, Pooled data from 40 bursts in four cells showing evoked burst duration before and after IBTX. $^{**}p < 0.01$. ***E***, Pooled data from four cells showing that IBTX (200 nM) does not affect LTSs recorded in current clamp in the presence of TTX (1 μM) and ZD7288 (100 μM). Inset, LTSs evoked by current steps before (control) and after (IBTX) 15 min of IBTX treatment. ***F***, Current-clamp recordings comparing burst duration before (black) and after (green) of ω-conotoxin MVIIC (CTxMVIIC) (5 μM; 10 min), a nonselective blocker of HVA Ca^{2+} channels, showing that burst duration is significantly lengthened by blocking HVA Ca^{2+} channels. Inset, Pooled data from five cells showing evoked burst duration before (control) and after ω-conotoxin MVIIC. $^{**}p < 0.01$. ***G***, Representative traces of the first three action potentials from evoked bursts before (black) and after IBTX (red; 200 nM; 15 min) or conotoxin MVIIC (green; 5 μM; 10 min) treatment, showing that the falling rather than the rising phases of action potentials are affected by blocking BK or HVA Ca^{2+} channels. ***H***, ***I***, Pooled data showing that IBTX ($n = 4$ cells) or conotoxin MVIIC ($n = 5$ cells) significantly reduces the decay slopes of the first three action potentials in each evoked burst. Error bars indicate SEM. $^{*}p < 0.05$; $^{**}p < 0.01$.

T- and/or L-type Ca^{2+} currents sustain the burst envelope

Ca^{2+} channels comprise two groups: HVA, with activation threshold more positive than approximately −30 mV, are further classified into L-, N-, P/Q-, and R-type based on their biophysical and pharmacological properties. LVA calcium channels, which activate at potentials more negative than approximately −45 mV (Catterall, 2000; Catterall et al., 2005), are traditionally considered as T-type Ca^{2+} channels.

ET cells have an LVA Ca^{2+} conductance with a calculated activation voltage of approximately −61 mV. This current has properties of both T- and L-type Ca^{2+} channels. Its pharmacology as well as its activation and inactivation kinetics suggest that it is mediated by T-subtype $Ca_V3.3$ (α1I) and/or L-subtype Cav1.3 (α_{1D}) Ca^{2+} channels, both of which are expressed in the glomerular layer at both mRNA and protein levels (Hell et al., 1993; Ludwig et al., 1997; Talley et al., 1999; Yunker et al., 2003).

An established role of LVA Ca^{2+} conductance is the generation of LTSs, which are typically crowned by a burst of action

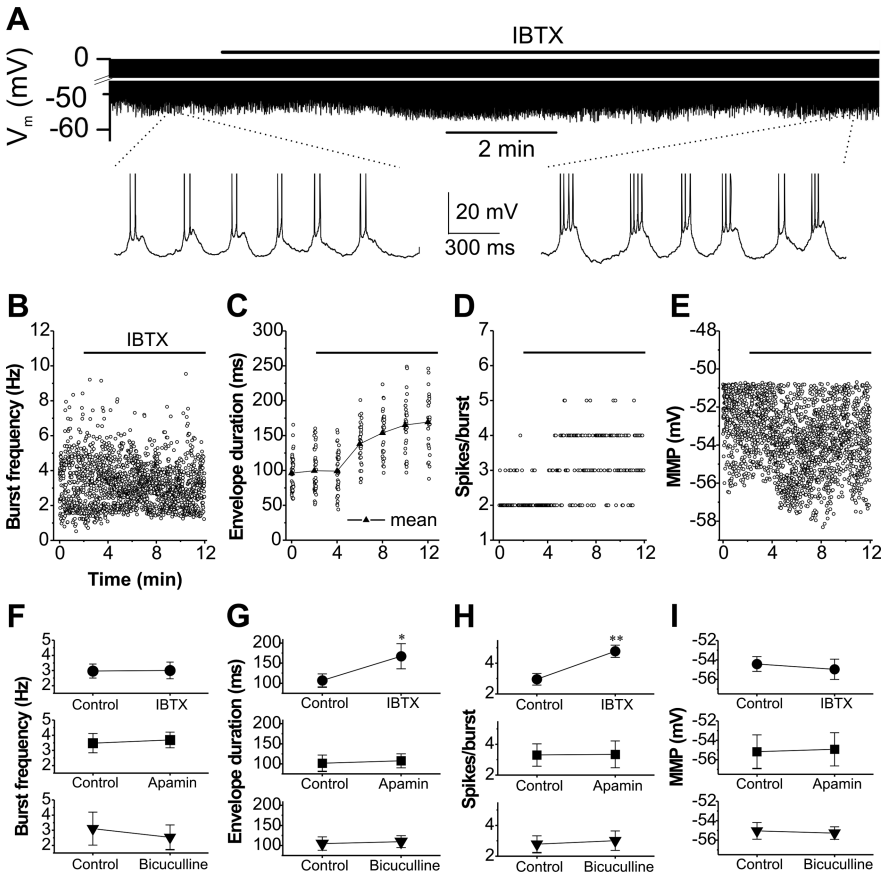

Figure 11. BK channels regulate spontaneous burst termination. ***A***, Current-clamp recording showing that IBTX (200 nM) increases both envelope duration and spikes per burst (traces below expanded timescale) of spontaneous bursting. ***B–E***, Graphs showing the effect of IBTX on burst frequency (***B***), depolarizing envelope duration (***C***), spikes per burst (***D***), and MMP (***E***) of the cell in ***A***. ***F–I***, Mean values of burst frequency, duration of depolarizing envelope, spikes per burst, and MMP from five cells before (control) and 10 min after IBTX; four cells before (control) and 10 min after apamin (300 nM), a specific SK channel blocker; and five cells before (control) and 10 min after bicuculline (30 μM), a blocker of apamin-insensitive SK channels, respectively. Error bars indicate SEM. *$p < 0.05$; **$p < 0.01$.

potentials (Perez-Reyes, 2003). LTSs could be evoked in all mouse ET cells and were abolished by both NNC 55-0396, and high doses of nimodipine, and were enhanced by Bay K8644. T-type channel blockade terminated spontaneous bursting, which indicates an essential role of I_T in the burst mechanism. Envelope duration and spikes per burst were both significantly increased by BayK. Nimodipine shortened but did not eliminate spontaneous bursting. This may be attributable to incomplete block of L-type channels by nimodipine at the dose (20 μM) used in the present study. Because higher doses of nimodipine produce nonselective effects on other types of Ca^{2+} channels, they were not tested (Randall and Tsien, 1997). Alternatively, T-type channels may contribute sufficient conductance to support bursting in the absence of L-type channels. It is also possible that T-type and L-type channels cooperate such that T-type channels are primarily involved in launching the burst envelope, whereas L-type channels provide an additional depolarizing boost and also prolong burst duration.

Role of BK conductance in burst termination

In addition to the generation of LTSs, Ca^{2+} currents elevate cytosolic Ca^{2+}, which can influence membrane conductances through Ca^{2+}-dependent channels. There is strong immunoreactivity for both BK and SK channels in the glomeruli (Sailer et al., 2004; Sausbier et al., 2006). Because of their very high single-channel conductance and activation dependence on both Ca^{2+} entry and membrane depolarization, BK channels provide an ideal negative-feedback mechanism that can potently regulate membrane excitability. The use of a selective blocker demonstrated for the first time that BK conductance is present in ET cells. The present study further revealed that activation of BK channels requires transient sodium current (I_{NaT})-mediated action potentials that increase intracellular Ca^{2+} via high-voltage activated Ca^{2+} channels. BK but not SK conductance plays an important role in terminating spontaneous bursts. After inactivation of I_T, the outward current generated by I_{BK} may override the residual inward currents attributable to I_{NaP} and/or I_L. The resulting hyperpolarization would deactivate these two inward currents and drive the membrane toward the MMP. Thus, I_{BK} is a key determinant of burst duration.

Multiple conductances cooperatively regulate spontaneous bursting in ET cells

Together, the present findings suggest that multiple conductances (Fig. 12) cooperate to generate spontaneous, autonomous rhythmical bursting in mouse ET cells. These intrinsic, voltage-gated conductances may function coordinately in the following way: I_{NaP}, which is active at MMP depolarizes the membrane potential toward the activation voltage of $I_{T/L}$. Activation of these Ca^{2+} currents cooperates with I_{NaP} to generate a depolarizing envelope, which triggers a burst of action potentials via transient Na^+ channels (I_{NaT}). Action potentials induce Ca^{2+} influx through high-voltage-activated Ca^{2+} channels (I_{HVA}), thus further increasing cytosolic Ca^{2+}. The combination of elevated intracellular Ca^{2+} and membrane depolarization activates I_{BK}, which terminates bursting and contributes to the repolarization of action potentials. The membrane hyperpolarization by I_{BK} activates the inward current I_h, which resets MMP and initiates the next burst cycle by cooperating with I_{NaP} to depolarize the cell membrane.

Three of these conductances, I_h, I_{NaP}, and I_T, have previously been implicated in burst generation in a wide variety of neurons (Crill, 1996; Huguenard, 1996; Pape, 1996; Perez-Reyes, 2003; Robinson and Siegelbaum, 2003). Spontaneous as well as network-dependent bursting is generally thought to involve T-type channels. L-type Ca^{2+} channels have not been reported to play a role in spontaneous bursting activity. A novel finding of the present study thus is that L-type Ca^{2+} channels play key roles in the autonomous bursting of ET cells. A second novel aspect of ET cell bursting is the role of BK channels. I_{BK} was hypothesized to play a role in fast rhythmic bursting in a multiconductance computational model of cortical pyramidal cells (Traub et al., 2003), but the present study provides the first experimental evidence that I_{BK} plays a key role in the mechanism of bursting. Our data indicate that I_{BK} regulates burst duration by terminating the de-

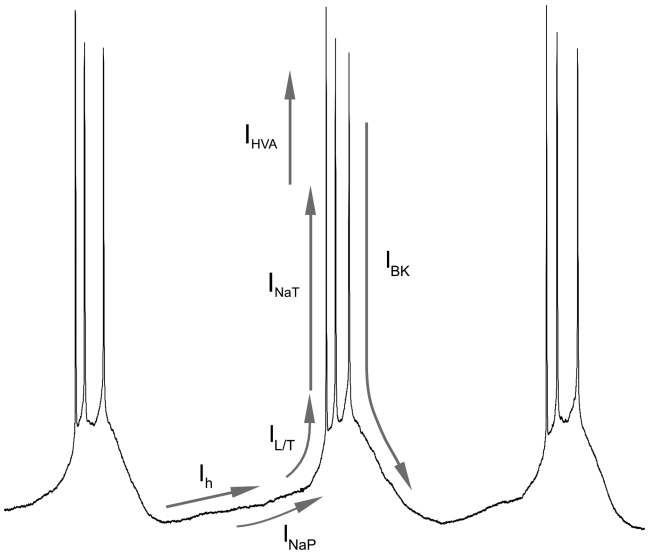

Figure 12. Multiple conductances cooperatively regulate bursting in ET cells. I_h is active at MMP. Depolarization produced by I_h increases the activation of persistent sodium channels (I_{NaP}), further depolarizing the membrane to the activation threshold(s) for L- and/or T-type Ca^{2+} channels, which trigger Ca^{2+} influx ($I_{L/T}$) and cooperate with I_{NaP} to evoke a depolarizing envelope. The depolarizing envelope activates transient sodium channels (I_{NaT}) generating a burst of action potentials. Action potentials open high-voltage activated (I_{HVA}) Ca^{2+} channels, which further increase cytosolic Ca^{2+} $[Ca^{2+}]_i$ concentration. The combination of increased $[Ca^{2+}]_i$ and membrane depolarization opens the large-conductance Ca^{2+}-dependent potassium channels, I_{BK}, which contributes to action potential repolarization, burst termination, and membrane hyperpolarization, thus reactivating I_h.

polarizing envelope. Indeed, these two currents may go hand-in-hand: The slow inactivation of I_L may necessitate the requirement of Ca^{2+}-voltage-dependent outward current such as I_{BK} to terminate the burst.

ET cells spontaneously burst in frequency range of 0.2–8 Hz (Hayar et al., 2004a). Each ET cell has its own stable intrinsic burst frequency within this range. The voltage-dependent conductances that regulate the burst cycle (I_{NaP}, $I_{T/L}$, I_{BK}, and I_h) did not express sufficient variability of strength or kinetics across cells to account for the 25-fold variability in interburst intervals exhibited by the ET cell population. Thus, an important question is what mechanism(s) determine the interval between burst cycles? One possibility is the involvement of slowly inactivating outward currents. The interplay between such currents and the opposing actions of I_h and I_{NaP} might account for variable interburst intervals and thus different autonomous bursting frequencies among different ET cells. This and other possible mechanisms await investigation.

Functional implications

ET cells play a pivotal role in glomerular circuitry. They receive monosynaptic ON inputs and provide monosynaptic glutamatergic input to SA and GABAergic PG cells (Hayar et al., 2004b). Thus, ET cells provide the principal sensory-evoked excitatory drive on the two major inhibitory circuits in the glomerular network: (1) the ON→ET→PG intraglomerular circuit, which inhibits postsynaptic targets in the same glomerulus; and (2) the ON→ET→SA→PG interglomerular circuit, which inhibits targets in distant glomeruli. Both circuits strongly determine how glomerular activity regulates information conveyed to more central olfactory targets by mitral/tufted cells (Aungst et al., 2003; Wachowiak and Shipley, 2006). Each of the conductances that regulate the ET cell burst cycle is subject to modulation (Nicoll et al., 1990) by neurotransmitters/neuromodulators present in glomeruli, including dopamine, serotonin, acetylcholine, and glutamate via mGluRs (metabotropic glutamate receptors) (Shipley et al., 2004). Modulation of these conductances could significantly influence intraglomerular and interglomerular inhibition and thus the impact of the olfactory bulb on higher levels of odor processing.

References

Antal M, Eyre M, Finklea B, Nusser Z (2006) External tufted cells in the main olfactory bulb form two distinct subpopulations. Eur J Neurosci 24:1124–1136.

Aungst JL, Heyward PM, Puche AC, Karnup SV, Hayar A, Szabo G, Shipley MT (2003) Centre-surround inhibition among olfactory bulb glomeruli. Nature 426:623–629.

Avery RB, Johnston D (1996) Multiple channel types contribute to the low-voltage-activated calcium current in hippocampal CA3 pyramidal neurons. J Neurosci 16:5567–5582.

Bezprozvanny I, Tsien RW (1995) Voltage-dependent blockade of diverse types of voltage-gated Ca^{2+} channels expressed in *Xenopus* oocytes by the Ca^{2+} channel antagonist mibefradil (Ro 40-5967). Mol Pharmacol 48:540–549.

Bourinet E, Stotz SC, Spaetgens RL, Dayanithi G, Lemos J, Nargeot J, Zamponi GW (2001) Interaction of SNX482 with domains III and IV inhibits activation gating of alpha(1E) (Ca(V)2.3) calcium channels. Biophys J 81:79–88.

Buzsaki G, Draguhn A (2004) Neuronal oscillations in cortical networks. Science 304:1926–1929.

Catterall WA (2000) Structure and regulation of voltage-gated Ca^{2+} channels. Annu Rev Cell Dev Biol 16:521–555.

Catterall WA, Perez-Reyes E, Snutch TP, Striessnig J (2005) International Union of Pharmacology. XLVIII. Nomenclature and structure-function relationships of voltage-gated calcium channels. Pharmacol Rev 57:411–425.

Crill WE (1996) Persistent sodium current in mammalian central neurons. Annu Rev Physiol 58:349–362.

Crunelli V, Toth TI, Cope DW, Blethyn K, Hughes SW (2005) The "window" T-type calcium current in brain dynamics of different behavioural states. J Physiol (Lond) 562:121–129.

Grunnet M, Kaufmann WA (2004) Coassembly of big conductance Ca^{2+}-activated K^+ channels and L-type voltage-gated Ca^{2+} channels in rat brain. J Biol Chem 279:36445–36453.

Hablitz JJ, Johnston D (1981) Endogenous nature of spontaneous bursting in hippocampal pyramidal neurons. Cell Mol Neurobiol 1:325–334.

Hayar A, Karnup S, Shipley MT, Ennis M (2004a) Olfactory bulb glomeruli: external tufted cells intrinsically burst at theta frequency and are entrained by patterned olfactory input. J Neurosci 24:1190–1199.

Hayar A, Karnup S, Ennis M, Shipley MT (2004b) External tufted cells: a major excitatory element that coordinates glomerular activity. J Neurosci 24:6676–6685.

Hayar A, Shipley MT, Ennis M (2005) Olfactory bulb external tufted cells are synchronized by multiple intraglomerular mechanisms. J Neurosci 25:8197–8208.

Hell JW, Westenbroek RE, Warner C, Ahlijanian MK, Prystay W, Gilbert MM, Snutch TP, Catterall WA (1993) Identification and differential subcellular localization of the neuronal class C and class D L-type calcium channel alpha 1 subunits. J Cell Biol 123:949–962.

Holderith NB, Shigemoto R, Nusser Z (2003) Cell type-dependent expression of HCN1 in the main olfactory bulb. Eur J Neurosci 18:344–354.

Huang L, Keyser BM, Tagmose TM, Hansen JB, Taylor JT, Zhuang H, Zhang M, Ragsdale DS, Li M (2004) NNC 55-0396 [(1*S*,2*S*)-2-(2-(*N*-[(3-benzimidazol-2-yl)propyl]-*N*-methylamino)ethyl)-6-fluoro-1,2,3,4-tetrahydro-1-isopropyl-2-naphtyl cyclopropanecarboxylate dihydrochloride]: a new selective inhibitor of T-type calcium channels. J Pharmacol Exp Ther 309:193–199.

Huguenard JR (1996) Low-threshold calcium currents in central nervous system neurons. Annu Rev Physiol 58:329–348.

Jinno S, Ishizuka S, Kosaka T (2003) Ionic currents underlying rhythmic bursting of ventral mossy cells in the developing mouse dentate gyrus. Eur J Neurosci 17:1338–1354.

Khawaled R, Bruening-Wright A, Adelman JP, Maylie J (1999) Bicuculline

block of small-conductance calcium-activated potassium channels. Pflügers Arch 438:314–321.
Koschak A, Reimer D, Huber I, Grabner M, Glossmann H, Engel J, Striessnig J (2001) alpha 1D (Cav1.3) subunits can form l-type Ca^{2+} channels activating at negative voltages. J Biol Chem 276:22100–22106.
Krnjevic K, Puil E, Werman R (1975) Evidence for Ca^{2+}-activated K^+ conductance in cat spinal motoneurons from intracellular EGTA injections. Can J Physiol Pharmacol 53:1214–1218.
Laurent G (2002) Olfactory network dynamics and the coding of multidimensional signals. Nat Rev Neurosci 3:884–895.
Li M, Hansen JB, Huang L, Keyser BM, Taylor JT (2005) Towards selective antagonists of T-type calcium channels: design, characterization and potential applications of NNC 55-0396. Cardiovasc Drug Rev 23:173–196.
Lipscombe D, Helton TD, Xu W (2004) L-type calcium channels: the low down. J Neurophysiol 92:2633–2641.
Lledo PM, Gheusi G, Vincent JD (2005) Information processing in the mammalian olfactory system. Physiol Rev 85:281–317.
Ludwig A, Flockerzi V, Hofmann F (1997) Regional expression and cellular localization of the alpha1 and beta subunit of high voltage-activated calcium channels in rat brain. J Neurosci 17:1339–1349.
Luthi A, McCormick DA (1998) H-current: properties of a neuronal and network pacemaker. Neuron 21:9–12.
Luthi A, Bal T, McCormick DA (1998) Periodicity of thalamic spindle waves is abolished by ZD7288,a blocker of Ih. J Neurophysiol 79:3284–3289.
Magee JC, Avery RB, Christie BR, Johnston D (1996) Dihydropyridine-sensitive, voltage-gated Ca^{2+} channels contribute to the resting intracellular Ca^{2+} concentration of hippocampal CA1 pyramidal neurons. J Neurophysiol 76:3460–3470.
Maher BJ, Westbrook GL (2005) SK channel regulation of dendritic excitability and dendrodendritic inhibition in the olfactory bulb. J Neurophysiol 94:3743–3750.
McDonough SI, Bean BP (1998) Mibefradil inhibition of T-type calcium channels in cerebellar purkinje neurons. Mol Pharmacol 54:1080–1087.
McDonough SI, Swartz KJ, Mintz IM, Boland LM, Bean BP (1996) Inhibition of calcium channels in rat central and peripheral neurons by ω-conotoxin MVIIC. J Neurosci 16:2612–2623.
Metz AE, Jarsky T, Martina M, Spruston N (2005) R-type calcium channels contribute to afterdepolarization and bursting in hippocampal CA1 pyramidal neurons. J Neurosci 25:5763–5773.
Milesi V, Aiello EA, Rebolledo A, Gomez AA, Grassi de Gende AO (1999) Role of a Ca^{2+}-activated K^+ current in the maintenance of resting membrane potential of isolated, human, saphenous vein smooth muscle cells. Pflügers Arch 437:455–461.
Monteggia LM, Eisch AJ, Tang MD, Kaczmarek LK, Nestler EJ (2000) Cloning and localization of the hyperpolarization-activated cyclic nucleotide-gated channel family in rat brain. Brain Res Mol Brain Res 81:129–139.
Murphy GJ, Darcy DP, Isaacson JS (2005) Intraglomerular inhibition: signaling mechanisms of an olfactory microcircuit. Nat Neurosci 8:354–364.
Nicoll RA, Malenka RC, Kauer JA (1990) Functional comparison of neurotransmitter receptor subtypes in mammalian central nervous system. Physiol Rev 70:513–565.
Notomi T, Shigemoto R (2004) Immunohistochemical localization of Ih channel subunits, HCN1–4, in the rat brain. J Comp Neurol 471:241–276.
Pape HC (1996) Queer current and pacemaker: the hyperpolarization-activated cation current in neurons. Annu Rev Physiol 58:299–327.
Park JY, Kang HW, Jeong SW, Lee JH (2004) Multiple structural elements contribute to the slow kinetics of the Cav3.3 T-type channel. J Biol Chem 279:21707–21713.
Perez-Reyes E (2003) Molecular physiology of low-voltage-activated t-type calcium channels. Physiol Rev 83:117–161.
Ramirez JM, Tryba AK, Pena F (2004) Pacemaker neurons and neuronal networks: an integrative view. Curr Opin Neurobiol 14:665–674.
Randall AD, Tsien RW (1997) Contrasting biophysical and pharmacological properties of T-type and R-type calcium channels. Neuropharmacology 36:879–893.
Robinson RB, Siegelbaum SA (2003) Hyperpolarization-activated cation currents: from molecules to physiological function. Annu Rev Physiol 65:453–480.
Sailer CA, Kaufmann WA, Marksteiner J, Knaus HG (2004) Comparative immunohistochemical distribution of three small-conductance Ca^{2+}-activated potassium channel subunits, SK1, SK2, and SK3 in mouse brain. Mol Cell Neurosci 26:458–469.
Santoro B, Chen S, Luthi A, Pavlidis P, Shumyatsky GP, Tibbs GR, Siegelbaum SA (2000) Molecular and functional heterogeneity of hyperpolarization-activated pacemaker channels in the mouse CNS. J Neurosci 20:5264–5275.
Sausbier U, Sausbier M, Sailer CA, Arntz C, Knaus HG, Neuhuber W, Ruth P (2006) Ca^{2+}-activated K^+ channels of the BK-type in the mouse brain. Histochem Cell Biol 125:725–741.
Shipley MT, Ennis M, Puche AC (2004) Olfactory system. In: The rat nervous system (Paxinos G, ed), pp 923–964. San Diego: Elsevier.
Talley EM, Cribbs LL, Lee JH, Daud A, Perez-Reyes E, Bayliss DA (1999) Differential distribution of three members of a gene family encoding low voltage-activated (T-type) calcium channels. J Neurosci 19:1895–1911.
Traub RD, Buhl EH, Gloveli T, Whittington MA (2003) Fast rhythmic bursting can be induced in layer 2/3 cortical neurons by enhancing persistent Na^+ conductance or by blocking BK channels. J Neurophysiol 89:909–921.
Tsien RW, Ellinor PT, Horne WA (1991) Molecular diversity of voltage-dependent Ca^{2+} channels. Trends Pharmacol Sci 12:349–354.
Wachowiak M, Shipley MT (2006) Coding and synaptic processing of sensory information in the glomerular layer of the olfactory bulb. Semin Cell Dev Biol 17:411–423.
Wilson RI, Mainen ZF (2006) Early events in olfactory processing. Annu Rev Neurosci 29:163–201.
Womack MD, Khodakhah K (2004) Dendritic control of spontaneous bursting in cerebellar Purkinje cells. J Neurosci 24:3511–3521.
Xu W, Lipscombe D (2001) Neuronal Ca(V)1.3alpha(1) L-type channels activate at relatively hyperpolarized membrane potentials and are incompletely inhibited by dihydropyridines. J Neurosci 21:5944–5951.
Young TA, Wilson DA (1999) Frequency-dependent modulation of inhibition in the rat olfactory bulb. Neurosci Lett 276:65–67.
Yunker AM, Sharp AH, Sundarraj S, Ranganathan V, Copeland TD, McEnery MW (2003) Immunological characterization of T-type voltage-dependent calcium channel CaV3.1 (alpha 1G) and CaV3.3 (alpha 1I) isoforms reveal differences in their localization, expression, and neural development. Neuroscience 117:321–335.
Zamponi GW, Bourinet E, Snutch TP (1996) Nickel block of a family of neuronal calcium channels: subtype- and subunit-dependent action at multiple sites. J Membr Biol 151:77–90.